

The Nature of Accreting Black Holes in Nearby Galaxy Nuclei

Edward J. M. Colbert ¹ and Richard F. Mushotzky

Laboratory for High Energy Astrophysics, Code 662, NASA/GSFC, Greenbelt, MD 20771

Received _____; accepted _____

¹NAS/NRC Research Associate

ABSTRACT

We have found compact X-ray sources in the center of 21 (54%) of 39 nearby face-on spiral and elliptical galaxies with available ROSAT HRI data. ROSAT X-ray luminosities (0.2 – 2.4 keV) of these compact X-ray sources are $\sim 10^{37} - 10^{40}$ erg s $^{-1}$ (with a mean of 3×10^{39} erg s $^{-1}$). The mean displacement between the location of the compact X-ray source and the optical photometric center of the galaxy is ~ 390 pc. The fact that compact nuclear sources were found in nearly all (five of six) galaxies with previous evidence for a black hole or an AGN indicates that at least some of the X-ray sources are accreting supermassive black holes. ASCA spectra of six of the 21 galaxies show the presence of a hard component with relatively steep ($\Gamma \approx 2.5$) spectral slope. A multicolor disk blackbody model fits the data from the spiral galaxies well, suggesting that the X-ray object in these galaxies may be similar to a Black Hole Candidate in its soft (high) state. ASCA data from the elliptical galaxies indicate that hot ($kT \approx 0.7$ keV) gas dominates the emission. The fact that (for both spiral and elliptical galaxies) the spectral slope is steeper than in normal type 1 AGNs and that relatively low absorbing columns ($N_H \approx 10^{21}$ cm $^{-2}$) were found to the power-law component indicates that these objects are somehow geometrically and/or physically different from AGNs in normal active galaxies. The X-ray sources in the spiral and elliptical galaxies may be black hole X-ray binaries, low-luminosity AGNs, or possibly young X-ray luminous supernovae. Assuming the sources in the spiral galaxies are accreting black holes in their soft state, we estimate black hole masses $\sim 10^2 - 10^4$ M $_{\odot}$.

Subject headings: galaxies: active — X-rays: galaxies

1. Introduction

An important unanswered question in extragalactic astronomy is whether supermassive black holes (BHs) exist in the nuclei of most galaxies. Since most galaxies are classified as “normal,” this question translates into: Are supermassive BHs present in the nuclei of most normal galaxies?

It is commonly accepted that galaxies with active galactic nuclei (AGNs) have nuclear BHs with masses $\sim 10^6$ – 10^9 M_\odot . However, “classical” AGNs represent only a small fraction of all galaxies. For example, Seyfert galaxies comprise $\sim 1\%$ of all luminous spiral galaxies (Osterbrock 1989). The geometrical model of AGNs is a supermassive black hole immediately surrounded by a hot accretion disk. Further out (\lesssim several pc), the hole and disk are encircled by an optically thick molecular torus (cf., Antonucci 1993). Optical spectra of AGNs show broad (~ 1000 km s $^{-1}$ FWHM) and “narrow” (several 100 km s $^{-1}$ FWHM) emission-line features from, respectively, the so-called broad-line region (BLR) located within ~ 0.1 pc, and the narrow-line region (NLR), which lies out to radii of several 100 pc. Convincing evidence for nuclear BHs in active galaxies comes from rotation curves of H₂O megamaser sources in the LINER galaxy NGC 4258 (Miyoshi et al. 1995) and rotation curves of a small, ionized gas disk in the nearby radio galaxy M87 (Ford et al. 1994; Harms et al. 1994).

There is considerably less known about the existence of supermassive BHs in normal galaxy nuclei. Dynamical searches for BHs in normal galaxies reveal central dark objects with masses $\sim 10^6$ – $10^{9.5}$ M_\odot in many nearby galaxies (cf. Kormendy & Richstone 1995), so it is feasible that many normal galaxies do contain nuclear supermassive BHs. However, normal galaxy nuclei do not show optical evidence for BLRs and NLRs and their optical/ultraviolet continua do not typically show the signature of the “big blue bump,” which is thought to be emission from the accretion disk in AGNs. One possible model

of galaxies purports that supermassive BHs are present in all galaxies, but are “active” in some and “inactive” in the others (e.g. Cavalieri & Padovani 1988). In this scenario, normal galaxies could be galaxies in which the BH/accretion disk is relatively “inactive.”

Why might supermassive BHs in normal galaxies be less luminous than AGNs in active galaxies? There are at least two possibilities. First, the mass of the BH may be significantly smaller ($M_{BH} \ll 10^6 M_{\odot}$). Second, the accretion rate may be much less (than in Seyfert galaxy AGNs, for example). It has been proposed by Narayan & Yi (1994, 1995a, 1995b) that accreting flows in BHs with low accretion rates are advection dominated (i.e., very little energy is radiated away during the accretion process). In this model for advection-dominated accretion flows (ADAFs), matter does not flow inwards in the form of a standard thin accretion disk, the flow pattern is closer to being spherical. An ADAF model fits the observed properties of the low-luminosity AGN NGC 4258, although a thin disk plus corona model is also allowed Lasota et al. 1996; Herrnstein et al. 1998; Gammie, Narayan & Blandford 1999). The X-ray emission from cores of elliptical galaxies is also well modelled by an ADAF and is consistent with central black hole masses of $\sim 10^9 M_{\odot}$ (Reynolds et al. 1997; Di Matteo & Fabian 1997 and references therein), as is observed for M87 (Ford et al. 1994; Harms et al. 1994).

X-ray emission from accreting BHs with standard thin accretion disks has a characteristic power-law spectrum, thought to be produced by Compton scattering of ultraviolet photons from the accretion disk (cf. Svensson 1996). ADAF accretion flows produce soft X-ray emission by Comptonization of synchrotron photons and hard X-rays via bremsstrahlung (Mahadevan 1997). Whether accreting BHs in normal galaxy nuclei are surrounded by a thin accretion disk or are advection-dominated, they should be associated with compact X-ray emission from regions immediately surrounding the BH, so compact X-ray sources are good indicators of nuclear BHs in galaxy nuclei. Only a few different

types of point sources in external galaxies emit at high enough fluxes so that present day X-ray observations can detect them: X-ray bright supernova remnants (cf. Schlegel 1995), luminous X-ray binaries, and luminous galactic nuclei. At other wavelengths (e.g., optical), there are much more possible sources of emission besides compact galactic nuclei. Therefore, X-ray observations are unique in their ability to identify accreting BHs in galactic nuclei.

As an example, consider the X-ray source in the nuclear region of the nearby normal galaxy NGC 1313. A bright X-ray source in the nuclear region of this galaxy is located ~ 1 kpc from the optical nucleus, has $L_X(0.2 - 2.4 \text{ keV}) \sim 10^{40} \text{ erg s}^{-1}$, implying a BH mass of $\sim 10^3 - 10^4 \text{ M}_\odot$ for an Eddington ratio of $10^{-2} - 10^{-1}$ (Colbert et al. 1995). There is no evidence for an AGN at wavelengths other than X-ray, yet the implied mass is much larger than those of typical BH X-ray binaries (XRBs) ($\sim 5 - 10 \text{ M}_\odot$, Tanaka 1989).

We seek to understand the nature of these near-nuclear compact X-ray sources. Do they represent a class of low-luminosity AGN perhaps similar to Seyfert nuclei, e.g. AGNs with advection-dominated accretion flows (ADAFs)? Or are they BH XRBs with BH masses of $\sim 10 - 10^4 \text{ M}_\odot$? Or are they a new class of object with properties yet to be discovered?

In the present paper, we describe the X-ray properties of compact X-ray sources in the nuclei of a sample of nearby normal galaxies, with the hope of determining the nature of the X-ray sources. In section 2, we describe the selection process for the sample, and in section 3 we describe the observations and data reduction technique. The results from the ROSAT HRI survey (of 39 galaxies) are presented in section 4 and the results from ASCA observations of six of those galaxies are presented in section 5. Possible scenarios for the origin of the compact X-ray sources are discussed in section 6. A summary of the results is given in section 7.

2. Sample Selection

Our goal was to select a sample of galaxies in which compact X-ray sources could be associated with accreting BHs as unambiguously as possible. By using data from the ROSAT HRI instrument, we choose the the best angular resolution X-ray data available for such a study. All galaxies with recessional velocities smaller than 1000 km s^{-1} were selected from an electronic version (vers. 3.9) of the *Third Reference Catalog of Bright Galaxies* (de Vaucouleurs et al. 1991;RC3). We omitted galaxies in which the disks were edge-on, since the additional large absorbing columns significantly lower the count rates of any potential X-ray sources and might produce low-quality spectra. More specifically, we required that the logarithm of the axial ratio be smaller than 0.4 (as taken from RC3). Starburst galaxies produce X-ray emitting galactic winds which extend out of the nuclear region and the nuclear starbursts themselves are sources of X-ray emission (often with very complex structure), so we chose to omit starburst galaxies from our sample. We deselected starburst galaxies by requiring L_{FIR} (calculated from IRAS fluxes using the method described in Fullmer & Lonsdale 1989) to be less than the blue B luminosity L_B . We then required that there be sufficiently good (exposure time $\gtrsim 3 \text{ ks}$) ROSAT HRI data available in the public archives, so that luminosities $\gtrsim 10^{39} \text{ erg s}^{-1}$ could be sampled. The Seyfert galaxy NGC 4151 was omitted from the sample since it is already known to have a bright X-ray emitting AGN. The Local Group galaxies SMC and LMC were also omitted from the sample since they project too large an area on the sky to make ROSAT imaging feasible without mosaicing. These selection criteria produced a list of 39 nearby galaxies (see Table 1).

EDITOR: PLACE TABLE 1 HERE.

3. Observations and Data Reduction

3.1. ROSAT HRI data

All available HRI data for the selected 39 galaxies were retrieved from the US ROSAT archives at NASA/GSFC. A list of the observational data used is given in Table 2, along with the exposure times. We used the IRAF/PROS software package to produce event list files, which were then used for imaging. All imaging data were first blocked by a factor of two to give 1" pixels, and were then smoothed with a Gaussian profile with $\sigma = 3''$. Contour maps of the smoothed images were overlayed on digitized B-band survey plate images (from the STScI digitized sky survey) in order to visualize the relative location of the compact X-ray sources with respect to the galaxy nucleus. We defined an X-ray source to be in the “center” of the galaxy (i.e., a nuclear source) if it was located within 2 arcminutes of the optical photometric center.

EDITOR: PLACE TABLE 2 HERE.

Count rates were calculated from the unsmoothed HRI images using circular source regions of radius 15", centered on the peak pixel. Background counts were taken from annular regions surrounding the source. It was necessary in a few cases to restrict the azimuthal angle of the background region so that there would not be any contamination from nearby sources.

For the galaxies M33, M81, NGC 4374, NGC 4406 and NGC 4552, diffuse X-ray emission was present in the nuclear region, i.e., in the circular source regions. This was determined by trying to fit radial profiles for all of the galaxies with a Gaussian plus a constant and examining the residual X-ray emission. All but these five galaxies were consistent with the HRI point-spread function. Since the background region also samples

the diffuse emission, the net count rate was partially corrected when we subtracted the normalized background counts from the source counts in the source region. The diffuse emission tends to fill the source regions more than it fills the background region, so there is still some contaminated emission accounted for in the net count rate.

For the galaxies with extended diffuse emission, we estimated the count rate from the pointlike component of the X-ray emission by modelling the radial profile from the HRI image. Radial profiles were extracted using the XIMAGE software and models were fit to the data using the QDP plotting package. We fit a model consisting of a Gaussian component for the point-spread function of the compact X-ray source, a King model for the extended X-ray emission, and a constant component for the background X-ray emission. We then integrated the Gaussian and King components out to a radius of $15''$ (the size of the circle used for extracting source counts from the HRI image) and these integrals were used to determine the fraction of the total source counts which were from the (Gaussian) point source. We found fractions of 0.373, 0.611, 0.151, 0.328 and 0.171 for M33, M81, NGC 4374, NGC 4406, and NGC 4552, respectively. The net count rates for these five galaxies were modified using these correction factors and fluxes and luminosities in this paper correspond to these corrected count rates.

The ROSAT HRI data for the individual galaxies was also checked for variability. XSELECT was used to extract light curves from the raw data using the same source regions described above. XRONOS was used to plot the light curves. Most of the light curves showed less than 50% variability, although two galaxies showed variability on scales of 50% or more (Ho II displayed \sim 50% variability on \sim 0.2 day time scales and NGC 5204 displayed \sim 100% variability on \sim 0.3 day time scales).

3.2. ASCA data

Data for eight observations (of six galaxies) in our sample were retrieved from the ASCA archives in order to facilitate our understanding of the nature of the compact X-ray sources. The six galaxies were selected because (1) they have compact X-ray sources in the HRI images, (2) no adjacent X-ray sources were present in the ASCA fields (so that the ASCA spectra include point-source and possible diffuse emission only from the galaxy under study), and (3) public archival ASCA data were available. A list of the ASCA observations is given in Table 3.

EDITOR: PLACE TABLE 3 HERE.

The raw (“unscreened”) ASCA data were screened using the XSELECT software program (part of the FTOOLS X-ray analysis software package) using the following restrictions. Only BRIGHT mode data were used with high, medium and low bit rates. The maximum angular deviation from the source was set at 0.01° , the angle from bright Earth was restricted to be greater than 20° , the minimum elevation angle was set at 5° for the GIS data and 10° for the SIS data, the minimum cutoff rigidity (COR) was set to be 6 GeV/c, the Radiation Belt Monitor was restricted to be below 200, and the SIS PIXL rejection threshold was set at 100, 75 and 50 for 1, 2 and 4 CCD modes, respectively.

Source counts were extracted using circular or polygonal regions with typical diameters of $\sim 6\text{--}8'$ (SIS) and $\sim 7\text{--}12'$ (GIS). For both observations of NGC 1313, the central (nearest to the nucleus) X-ray source fell near the corner of the SIS CCD chip and polygonal regions with diameters $\sim 4\text{--}5'$ were used to extract source counts. Consequently, the SIS fluxes for NGC 1313 include a fraction (estimated $\gtrsim 60\%$ from the ASCA point spread function) of the total emission from the source. Background counts were taken from source-free polygonal regions surrounding the source regions. For the SIS spectra, background counts

were taken from a region of the same CCD in which the source was located. Extended X-ray emission was noticed in the GIS image of NGC 4406, thus the source counts for that galaxy include some of the emission from this extended X-ray source.

4. Results from ROSAT HRI Observations

4.1. Notes on Individual Galaxies

Here we list notes for each of the 39 galaxies in the sample. The galaxies are organized in three different groups: dwarf galaxies, spiral and irregular galaxies, and elliptical and lenticular galaxies.

4.1.1. Dwarf Galaxies

NGC 205 (M110) – This is a normal dwarf galaxy and is one of the two elliptical companions to M31. There is no previous evidence for a central black hole and we do not detect a compact X-ray source.

NGC 221 (M32) – M32 is the other normal dwarf elliptical galaxy that is a companion to M31. Eskridge, White & Davis (1996) analyzed the ROSAT PSPC data for M32 and concluded that the emission from the central source could be due to either low-mass X-ray binaries or accretion onto a massive central black hole. Loewenstein et al. (1998) argue that the central source is most likely a single X-ray binary rather than an AGN, based on the presence of an offset of the compact X-ray source (offset = 33.6 pc, from our HRI image) with respect to the nucleus and extremely large intensity variations (from ASCA observations). Previous evidence for a central black hole of mass $10^{6.5} M_{\odot}$ comes from dynamical evidence (e.g., Bender et al. 1996).

NGC 1705 – Lamb et al. (1985) suggest that this dwarf galaxy is in a starburst or post-starburst phase. NED lists its classification as an H II region galaxy. We did not detect any compact X-ray sources in the nuclear region of NGC 1705.

Ho II – This dwarf Irr galaxy is a companion to M81. We found a bright compact X-ray source approximately 2 arcminutes to the east of the galaxy center.

ESO 495-G21 (He 2-10) – ESO 495-G21 was originally discovered as a planetary nebula (He 2-10) and is now known as a dwarf emission-line galaxy. We find a compact X-ray source coincident with the nucleus.

UGC 5086 – We did not detect any X-ray emission from this dwarf Irr galaxy.

Ho IX – This is a dwarf Irr galaxy and is a companion to M81. We did not find any X-ray emission from this galaxy.

Leo A – This dwarf Irr galaxy is a possible member of the Local Group. We did not find any X-ray emission from this galaxy.

IC 3303 – We found no X-ray emission from this dwarf spiral galaxy.

NGC 4627 – NGC 4627 is a dwarf elliptical galaxy and is a nearby companion to the edge-on spiral galaxy NGC 4631. We did not find any X-ray emission from NGC 4627.

NGC 5204 – This dwarf galaxy is labeled as having an H II region nucleus by HFS95. We find a compact X-ray source offset 17.3" (403 pc) from the nucleus.

4.1.2. Spiral and Irregular Galaxies

NGC 300 – This is a normal spiral galaxy similar to M33 in appearance, located in the Sculptor group. We did not find any compact X-ray sources within 1' of the nucleus of

NGC 300.

NGC 598 (M33) – M33 is a normal spiral galaxy in the Local Group. Of all of the galaxies in the Local Group, it has the most luminous X-ray nucleus. Recently Dubus et al. (1997) have found evidence for 106-day periodic variability of the nuclear X-ray source and argue that the source is a black hole X-ray binary with a $\sim 10 M_{\odot}$ primary (for an Eddington ratio of unity). The ASCA spectra of the central X-ray source have been analyzed by Takano et al. (1994). We discuss ASCA observations of this X-ray source in section 5.

NGC 1313 – NGC 1313 is a nearby normal spiral galaxy with many H II regions. Colbert et al. (1995) found that the central bright X-ray source was offset ~ 1 kpc from the photometric center, from analysis of ROSAT PSPC data. They argued that the X-ray source was an accretion-powered black hole of mass $\sim 10^3 - 10^4 M_{\odot}$ (for an Eddington ratio $\sim 10^{-2} - 10^{-1}$), but unlike an AGN since there is no evidence for a BLR, NLR or accretion disk. ASCA observations of the central X-ray source in this galaxy are discussed in section 5. A previous analysis of one of the ASCA observations was published in Petre et al. (1994).

AM 0337-353 – This galaxy is a normal spiral galaxy, also located in the Fornax cluster. We did not detect any compact X-ray sources in the nuclear region of AM 0337-353.

IC 342 – IC 342 is a large, face-on spiral galaxy with a normal galaxy nucleus. We found several compact X-ray sources in IC 342, one of which was coincident with the galaxy nucleus. ASCA observations of IC 342 are unable to isolate the central X-ray source seen in the ROSAT HRI image from other surrounding X-ray sources in the galaxy (Okada et al. 1994). However, Okada et al. (1998) suggest that another X-ray source (not the most central one) in the central regions of IC 342 may be an accreting BH of mass $\sim 100 M_{\odot}$.

NGC 2403 – NGC 2403 is a nearby spiral galaxy with similar global properties to M33 (Thornley 1996). The galaxy has many H II regions, but the nucleus seems quiescent (Beckman et al. 1987). A compact X-ray source we found was near (offset = 17.1''), but not coincident with the galaxy nucleus.

NGC 3031 (M81) – This galaxy is described as having a LINER nuclear spectrum (Heckman 1980); some nuclei classified as LINERs are low-luminosity AGNs (e.g., Ho, Filippenko, & Sargent 1994, hereafter HFS95). Petre et al. (1993) describe its X-ray spectrum as being similar to that of other LINERs with broad H α emission, but argue against the presence of an accretion disk. Ishisaki et al. (1996) argue for the presence of a low-luminosity AGN in M81, based on the results from eight ASCA observations.

UGCA 276 – We found no X-ray emission from this Irr galaxy.

UGC 7356 – We found no X-ray emission from this Irr galaxy.

NGC 4286 – No X-ray emission was found from this nearby spiral galaxy.

NGC 4449 – This is a Magellanic Irr galaxy with many H II regions and is undergoing active star formation (Bothun 1986). We found multiple compact X-ray sources in this galaxy, none of which is coincident with the galaxy center. The nearest X-ray source to the nucleus is located 39.3'' (572 pc) from the nucleus.

NGC 4485 – This Irr galaxy is tidally interacting with NGC 4490. HFS95 classify it as having an H II region nucleus. We detect very faint emission that is offset 20.5'' (924 pc) from the galaxy center.

NGC 4569 (M90) – This spiral galaxy is in the Virgo cluster. HFS95 label it as having a transition (LINER/H II) type nucleus. We find a compact X-ray source coincident with the nucleus.

NGC 5408 – NGC 5408 is an Irr galaxy. We detected a compact X-ray source offset 49.3" (1.2 kpc) from the galaxy center. We discuss the ASCA spectra of this X-ray source in section 5.

NGC 6822 – NGC 6822 is an Irr galaxy in the Local Group. We detected a compact X-ray source offset 28.4" (96.4 pc) from the galaxy center.

NGC 6946 – This is a face-on spiral galaxy which has an H II region nucleus (HFS95). We find several compact X-ray sources associated with NGC 6946, the closest one to the nucleus being coincident (offset < 10") with the galaxy nucleus.

NGC 7320 – This is the brightest spiral galaxy in Stephan's quintet. We did not find any X-ray emission from NGC 7320 (see also Pietsch et al. 1997).

4.1.3. Elliptical and Lenticular Galaxies

NGC 1396 – This galaxy is a normal lenticular/elliptical galaxy located in the Fornax cluster. We did not detect any compact X-ray sources in the nuclear region of NGC 1396.

NGC 3990 – NGC 3990 is a lenticular galaxy. We found no X-ray emission from this galaxy.

NGC 4138 – This spiral galaxy has a nucleus classified as "S1.9" by HFS95. However, we found no X-ray emission from NGC 4138.

NGC 4150 – NGC 4150 is a nearby, small lenticular galaxy. We found a compact X-ray source offset by 16.3" (767 pc) from the galaxy nucleus.

NGC 4190 – NGC 4190 is another nearby, small lenticular galaxy. The compact X-ray source we found is located 7.4" from the optical galaxy center.

NGC 4278 – This is a nearby elliptical galaxy with large-scale radio emission (Wrobel & Heeschen 1984). NED lists its classification as a Seyfert 1 galaxy and HFS95 classify its nucleus as having a LINER spectrum. We find a compact X-ray source coincident with the galaxy nucleus.

NGC 4374 (M84) – M84 is a classical example of a radio galaxy (cf. Bridle & Perley 1984) and is hosted by a giant elliptical galaxy. We find an X-ray source coincident with the nucleus and also find diffuse X-ray emission surrounding the nuclear X-ray source. The ASCA spectra of this X-ray source are discussed in section 5.

NGC 4387 – This elliptical galaxy did not have any detectable X-ray emission.

NGC 4406 (M86) – M86 is a bright elliptical galaxy in the Virgo cluster. We find a weak nuclear X-ray source and also detect the plume of diffuse X-ray emission extending toward the northwest (Forman, Jones & Tucker 1985). We discuss the ASCA spectra of this galaxy in section 5.

IC 3540 – We did not find any X-ray emission from this S0 galaxy.

NGC 4552 (M89) – This elliptical galaxy is also quite a bright radio source (Wrobel & Heeschen 1984). HFS95 label it as a transition object. We find a central compact X-ray source coincident with the nucleus, surrounded by diffuse X-ray emission. The ASCA spectra of this source are discussed in section 5.

4.2. Overview of Results from HRI survey

Of the 39 galaxies for which HRI imaging data were available, we found (detection $> 3\sigma$) compact X-ray sources within $\sim 2'$ of the nucleus of 21 galaxies. Lira, Lawrence & Johnson (1998) find a similar result. Here we have used the optical position listed in RC3

(the photometric center) as the location of the nucleus. Estimated uncertainties in the optical positions are given in RC3 as $0.^s1$ and $1''$. Upper limits (3σ) for the galaxies in which no sources were found are listed in Table 4. The X-ray sources in the 21 galaxies in which compact sources were detected are listed in Table 5.

EDITOR: PLACE TABLE 4 HERE.

EDITOR: PLACE TABLE 5 HERE.

In Table 5, we list the X-ray position of the compact X-ray source, the offset of the X-ray position from the photometric center, the HRI net count rate, and Galactic absorption column in the direction of the X-ray source. Also listed are (unabsorbed, e.g., corrected for Galactic absorption) 0.2–2.4 keV X-ray fluxes and luminosities of the X-ray source, assuming a power-law (photon index $\Gamma = 1.7$) spectrum and absorption from the Galactic hydrogen column. Note that the count rates, X-ray fluxes and luminosities for the galaxies with extended emission (M33, M81, NGC 4374, NGC 4406, and NGC 4552) have been corrected so that they reflect only the contribution from the point-like X-ray component (see section 3.1).

4.3. Host Galaxy Type

The host galaxies of the compact X-ray sources range from dwarf irregular to elliptical to spiral. We show histograms of the host galaxy type (from RC3) in Figure 1. The upper panel corresponds to galaxies in our sample with detected compact X-ray sources, while the lower panel corresponds to all galaxies in our sample. Elliptical galaxies have galaxy types -6, -5 or -4, lenticular galaxies -3, -2, or -1, spirals 0 ... 9, and irregulars 10, 11

and 90. One galaxy (ESO 495-G21, $T = 90.0$) has been omitted from the histogram for clarity. Although there seems to be a slight preference for the X-ray sources to be found either in late-type spirals and irregular galaxies, or elliptical galaxies, as can be seen in the lower plot, our sample is abnormally deficient in early-type spiral galaxies. Histograms for complete samples from RC3 are flat across galaxy T-type (e.g., Buta et al. 1994).

EDITOR: PLACE FIGURE 1 HERE.

4.4. X-ray Luminosities

A histogram of the 0.2–2.4 keV luminosities is shown in Figure 2. Luminosities of the compact sources ranged from 8×10^{36} erg s $^{-1}$ to $\sim 10^{40}$ erg s $^{-1}$, with a mean of 3×10^{39} erg s $^{-1}$. For reference, Seyfert galaxies typically have $L_X \sim 10^{42}–10^{44}$ erg s $^{-1}$ and the Eddington luminosity of a $1.4 M_\odot$ accreting neutron star is $10^{38.3}$ erg s $^{-1}$. So, on average, the X-ray sources are at least one order of magnitude more luminous than the most luminous (i.e., Eddington ratio of unity) neutron star X-ray binaries, but are several orders of magnitude less luminous than typical AGN in Seyfert nuclei.

Also shown in Figure 2 are the galaxy types of the host galaxies. Note that the most luminous X-ray sources ($L_X \sim 10^{40}$ erg s $^{-1}$) tend to be found in elliptical hosts.

EDITOR: PLACE FIGURE 2 HERE.

4.5. Separation from Galaxy Center

As can be noted from the entries in Table 5, the offsets of the X-ray sources from the galaxy nucleus (photometric center) is significant in many of the sources. In Figure 3, we

show a histogram of the angular separation between the X-ray source and photometric center. An interesting result of our study is that $\sim 40\%$ (9 of 21) of the compact sources were located $\gtrsim 10''$ ($\gtrsim 0.3$ kpc at the mean distance of our sample) from the photometric optical center (as listed in RC3). For comparison, most observed objects have ROSAT X-ray positional errors of $\lesssim 10''$ (Briel et al. 1996).

EDITOR: PLACE FIGURE 3 HERE.

In Figure 4, we show a plot of L_X vs. the angular separation between the X-ray source and the photometric center. It is noteworthy that the mean luminosity of sources with small ($\lesssim 200$ –400 pc) separation is similar to the mean luminosity of sources with large separation ($\gtrsim 200$ –400 pc; see also section 6.2.2).

EDITOR: PLACE FIGURE 4 HERE.

5. Results from ASCA Spectral Fitting

As noted previously, ASCA spectra were extracted for six galaxies in the sample (see Table 3). We attempted to fit several spectral models to the data using all four ASCA instruments (SIS0, SIS1, GIS2 and GIS3) simultaneously. We allowed the relative normalization of SIS1, GIS2 and GIS3 (with respect to SIS0) to vary while fitting each model. We ignored data from spectral bins marked “bad” by the XSELECT program as well as data from energy bins below 0.4 keV and above 10.0 keV.

We first tried fitting the data with two single component models: (1) a Raymond-Smith (RS) thermal plasma (Raymond & Smith 1977), as would be expected if the source were hot gas, and (2) a power-law (PL) model, as might be expected from an AGN or other

object accreting matter onto a BH via an accretion disk. The results from these fits are listed in Table 6. We list the spiral and elliptical galaxies separately since elliptical galaxies often show evidence for a strong component of hot gas (e.g. Forman et al. 1979), while spiral galaxies do not necessarily show such evidence.

EDITOR: PLACE TABLE 6 HERE.

A cursory look at the results in Table 6 shows that the power-law model is a better fit, in general, to the X-ray sources in the spiral galaxies, whereas the Raymond-Smith plasma model is a better fit for the elliptical galaxy sources. The power law fit for the elliptical galaxies is so poor for NGC 4374 and NGC 4406 that the reduced χ^2 values are greater than 2.0, which is too poor to be able to use χ^2 fitting to deduce standard errors for the parameters. It is immediately noticeable that the first observation of NGC 1313 gives a much different fit than for the second observation of NGC 1313. Most of the spiral galaxy sources are fit by a steep power law with $\Gamma \approx 2.3 - 2.8$ or a thermal plasma with $kT = 2.0 - 3.4$ keV. However, in the first observation of NGC 1313, the X-ray source is best fit with a significantly shallower power-law spectrum ($\Gamma = 1.7$) or a hotter Raymond-Smith plasma with $kT = 6.7$ keV.

The single-component fits to the elliptical galaxy sources are much poorer than those to the spiral galaxy sources, with $\chi^2_\nu > 1.5$ for five out of six fits. On the other hand, the single-component fits to the spiral galaxy sources are acceptable in nearly all cases, with $\chi^2_\nu > 1.2$ for only two out of ten fits.

We also tried modelling the data with multiple-component fits, for example with a RS+PL model (as appropriate for a BH embedded in diffuse gas, e.g., Ptak et al. 1998), and a disk blackbody (DBB, Mitsuda et al. 1988) plus power-law model (DBB+PL, as is seen in Galactic BH candidates). For the RS+PL model, the RS component was assumed to only

be absorbed by gas in our Galaxy (for Galactic columns, see Table 5), while absorption to the PL component was allowed to be larger. For the DBB+PL fit, the absorption to both components was assumed to be the same and was allowed to be larger than the Galactic value. The results from these fits are shown in Table 7.

EDITOR: PLACE TABLE ?? HERE.

We also list in Table 7 the values of the F statistic, comparing the single-component fits to the two-component fits. In nearly all cases, the two-component fits are preferred with very low probabilities of exceeding the F values by chance (significance of the extra terms $\gtrsim 97 - 99.9\%$). An exception is M33, in which the single component Raymond-Smith thermal plasma model is nearly equally as good a fit as the DBB+PL model. It should be noted here that the presence of a second (hard) component in X-ray spectra of elliptical galaxies has previously been discovered in ASCA spectra by Matsushita et al. (1994).

It is worthwhile to note that the elliptical galaxies are much better fit by a RS+PL model compared to a DBB+PL model, indicative of a hot gas component which is known to be common in these galaxies. Furthermore, the DBB fits to the elliptical galaxies gave very large values for the inner radius of the accretion disk ($r_{in}(\cos \theta)^{\frac{1}{2}}$) and imply considerably steeper power-law indices (compared to those from the RS+PL fits) and very low values of kT_{in} (the temperature at the inner radius of the accretion disk). This suggests that the DBB+PL model is incorrect for the elliptical galaxies and another component (or a different component) is needed to fit the spectra. For these reasons, we tried an additional three-component model consisting of a Raymond-Smith thermal plasma, a DBB, and a power-law model. The results of these fits are given in Table 8.

EDITOR: PLACE TABLE ?? HERE.

The values of the F-statistic for comparison with the two-component fits are also listed in Table 8. As can be seen from these values, the RS+DBB+PL fits are significantly better fits than the DBB+PL fits, but are not significantly preferred over the RS+PL models. Thus, we conclude that a disk blackbody component is not required by the spectral data and the RS+PL fits are the best fit models for the elliptical galaxies in our sample.

We should also note that for two (NGC 4406 and NGC 4552) of the three elliptical galaxies, the GIS spectra have higher normalization values than the SIS spectra (by mean values of 1.9 and 1.5, respectively). Since the GIS extraction regions are larger than those for the SIS, this implies that there is an extended component of X-ray emission, most likely a hot thermal plasma which we have modelled with a Raymond-Smith component. The ROSAT HRI images of these galaxies confirm that extended X-ray emission is present surrounding the central X-ray source (section 4.1).

The power-law slopes for the elliptical galaxy RS+PL models are considerably steeper than found for ASCA analysis of type 1 AGN, in which $\langle \Gamma \rangle = 1.91 \pm 0.07$ (Nandra et al. 1997). The mean value and standard deviation for our three elliptical galaxies is 2.55 ± 0.76 . This may be indicative of a different kind of emission process, for example both Narrow-Line Seyfert 1 galaxies and BH XRBs in their soft state have comparably steep power-law slopes.

We next turn to the three spiral galaxies in our ASCA sample. M33 is best fit by a DBB+PL model (as previously noted by Takano et al. 1994), although a RS+PL model is also allowed statistically (χ^2_ν values of 0.98 and 1.00 for the two separate observations). NGC 1313 and NGC 5408 are nearly equally well fit by either a RS+PL model or a DBB+PL model (the RS+PL model yields a slightly better fit).

Again, it is noteworthy that the power-law slopes for the spiral galaxies are also comparatively steep when compared with ASCA spectra of Seyfert 1 galaxies.

We next discuss the results of the spiral galaxy spectra in terms of emission expected from an BH XRB. In the hard state, BH XRBs typically have hard spectra with power-law slopes $\Gamma \approx 1.3 - 1.9$, whereas in the soft state, the power-law slope steepens to ≈ 2.5 (e.g., Ebisawa, Titarchuk, & Chakrabarti 1996) and a soft component appears in the X-ray spectrum (usually modelled as a multicolor disk blackbody component). The first observation of NGC 1313 exhibits a slope more consistent with a BH XRB in its hard state, while in the second observation the slope steepens to > 2.5 , more consistent with a soft state.

For the spiral galaxy X-ray sources, the values of the inner radius of the accretion disk (as predicted by the multicolor disk blackbody model) are given in Table 9. For M33, $r_{in}(\cos \theta)^{\frac{1}{2}}$ (≈ 40 km) is more consistent with values for BH candidates ($\approx 20 - 30$ km) than for low-mass X-ray binaries (LMXBs) ($\approx 5 - 10$ km; e.g., Yaqoob, Ebisawa, & Mitsuda 1993). The second observation of NGC 1313 (for which a steep spectral slope suggests a soft state) also yields a value of $r_{in}(\cos \theta)^{\frac{1}{2}}$ (≈ 30 km), consistent with a BH candidate. However, for NGC 5408, a significantly larger inner radius ($r_{in}(\cos \theta)^{\frac{1}{2}} \approx 18000$ km) is predicted. For comparison, the Schwarzschild radius $2GM/c^2$ of a $10^3 M_{\odot}$ BH is equal to 2950 km). Although we cannot show that the objects in these galaxies exhibit XRB-like emission, we can say that if the X-ray emission is disk blackbody emission from an XRB-like accretion disk in its soft state, the inner radii imply that the objects are BH candidates.

EDITOR: PLACE TABLE 9 HERE.

To further investigate the hypothesis that the emission is from XRB-like objects in their soft state, we fitted the spectra from the spiral galaxies with the bulk-motion (BM) model promoted by Titarchuk and collaborators (e.g., see Shrader & Titarchuk 1998). As

in the DBB+PL model, in this model, the soft X-ray photons are assumed to come directly from the thin accretion disk, whereas the hard photons come from upscattering of the soft photons by bulk motion and from downscattering of harder photons by Comptonization. Results from these fits are shown in Table 10.

EDITOR: PLACE TABLE 10 HERE.

In general, the fits were acceptable, although the reduced χ^2 values were typically higher than those for the RS+PL and DBB+PL fits. Again, the power-law slopes predicted by the BM model are quite steep (~ 2.5 , except for NGC 1313 observation 1, which seems to be in a hard state). Such steep slopes are consistent with a BH XRB in its soft state.

The normalization parameter from fitting the Bulk Motion model allows us to directly estimate the masses of the central BH. We list those predicted masses in Table 9. Note that for M33 and NGC 1313#2, these calculations imply BH candidates with masses $\gtrsim 10^2 M_\odot$. For NGC 5408, the predicted mass of the BH is $\sim 10^4 M_\odot$. We find that the best fit value of $r_{in}(\cos \theta)^{\frac{1}{2}}$ (from the DBB+PL models; Table 9) is less than the corresponding r_g for with the mass predicted by the BM models. We discuss this further in section 6.5.

We note that for the spiral galaxies, the DBB+PL model requires an additional (above that for our Galaxy) absorbing column of $N_H \sim 1-3 \times 10^{21} \text{ cm}^{-2}$. The RS+PL model also requires an additional absorbing column for M33 and NGC 1313 ($\sim 5-10 \times 10^{21} \text{ cm}^{-2}$). For NGC 5408, the best fit external absorbing column is 0, although it is poorly constrained and may be as high as $0.4 \times 10^{21} \text{ cm}^{-2}$ (90% confidence limit).

For the elliptical galaxies, the best fit model (RS+PL) also requires an additional absorbing column over the Galactic value (for the power-law component). The best fit values range from $\sim 3-7 \times 10^{21} \text{ cm}^{-2}$.

Note that for the BM fits to the spiral galaxies, essentially no intrinsic absorbing column is required, unlike the fits including DBB or RS components. We attribute this to the fact that the BM model uses a single blackbody to model the disk while the disk is usually modelled as a multiple-component blackbody (DBB model). Since a single blackbody model turns over at low energies, it mimics a DBB model with absorption at low energies and less absorption will be required.

6. Discussion

In order to investigate the nature of accreting BHs in nearby galaxy nuclei, we have searched for compact X-ray sources using ROSAT HRI and ASCA observations of a distance-limited sample of nearby galaxies. Before discussing the origin of the compact X-ray sources in the elliptical and spiral galaxies, we list some possible explanations for what the sources may be.

6.1. Possible Explanations for the Compact X-ray Sources

The compact X-ray sources could be AGN-like sources that for some reason do not reside in the nucleus, very luminous XRBs that are by chance located near the nucleus, superluminal X-ray transients, bright young X-ray supernovae, or some new, unexplained type of X-ray source.

6.1.1. Low-luminosity AGNs

As noted in section 4.4, the ROSAT soft X-ray luminosities of the compact X-ray sources are several orders of magnitude less luminous than typical Seyfert galaxies. Thus, if

the sources are AGNs, one would expect this difference to be due to either a lower BH mass (e.g., if the BH mass scales with X-ray luminosity, M_{BH} may be as low as $\sim 10^4 M_{\odot}$) or a lower accretion rate. If the mass accretion rate is low enough, the standard thin disk model for accretion (Shakura & Sunyaev 1973) is not required and the ADAFs become possible solutions (Narayan & Yi 1994).

Lasota et al. (1996) have used an ADAF model to explain the spectrum of the low-luminosity AGN NGC 4258. In their model, the outer disk is a standard optically thick thin accretion disk, but at smaller radii their model consists of an advection-dominated flow. It is consistent that mass accretion rates are low in low-luminosity AGNs. For example, L/L_{Edd} is estimated to be $\sim 10^{-4}$ for the LINER galaxy NGC 4258 (Lasota et al. 1996), when nominal values for classical AGNs are taken to be $\sim 10^{-3} - 10^{-2}$ (e.g., Wandel 1991).

6.1.2. Black Hole X-ray Binaries

Another possibility is that the compact X-ray sources are extraluminous X-ray binaries, e.g., X-ray binaries with primaries with mass $\gtrsim 10 M_{\odot}$ so that the Eddington luminosities are $\gtrsim 10^{39} \text{ erg s}^{-1}$, which is in the range of the soft X-ray luminosities of the compact X-ray sources in our sample of galaxies. This explanation would make it easier to understand why such a large fraction of the compact X-ray sources are displaced from the galaxy nucleus.

At some level, there is little difference between a massive BH binary (with $M_{BH} > 10 M_{\odot}$) and an AGN with a low-mass ($M_{BH} \ll 10^6 M_{\odot}$) BH. Both objects are expected to have accretion disks surrounding BHs of mass $\sim 10 - 10^4 M_{\odot}$.

ADAFs are also possible explanations for the X-ray emission in various stages of X-ray binaries (e.g., Narayan 1997). In low and quiescent states, $\dot{m} < \dot{m}_{crit}$ and the inner accretion disk is replaced with an ADAF. If the accretion rate increases (high states), the

standard thin disk and corona replace the ADAF and the X-ray luminosity increases.

BH binaries are typically found in one of two states (in general terms). In the first (soft, or high) state, the spectrum consists of a relatively steep ($\Gamma \approx 2.5$) power-law at high ($E \gtrsim 3$ keV) energies, and a soft “blackbody” like component seen below ~ 2 keV. BH binaries in their hard (low) state have power-law spectra with shallower slopes ($\Gamma \approx 1.3–1.9$) and no soft component. As noted in section 5, the spectral slopes of the objects in the ASCA sample are more consistent with BH X-ray binaries in their soft state. Note that since we have a flux-limited sample, we will preferentially select X-ray binaries which are in their most luminous state (the high/soft state).

6.1.3. *Superluminal X-ray Sources*

We note that there are two recently-discovered BH candidates in our own galaxy, GRS 1915+105 and GRO J1655+40, which show evidence of bipolar superluminal outflows in radio images. Although their X-ray luminosities are not much more than a few 10^{38} erg s $^{-1}$, it is possible that if the sources were beamed into the line of sight, luminosities $\gtrsim 10^{39}$ erg s $^{-1}$ (which is comparable to the luminosities we find for our compact X-ray sources) may be attained. An argument against these sources being responsible for most of the compact X-ray sources is that they are highly variable (e.g., Belloni et al. 1997), and it is not clear how frequently the sources would be in their “high” state.

Continuous observations with BATSE in the 20 keV – 2 MeV energy range show the superluminal X-ray transient GRS 1915+105 to be in a “high” state for periods up to one year in duration (Harmon et al. 1997). ROSAT and ASCA observations of these sources are, however, not as complete (e.g. Greiner 1996; Zhang et al. 1997), so the long-term behavior of the soft X-ray emission is not as well known. Based on the BATSE levels, the

flux seems to drop by a factor of up to 50 in the “low” state. If the objects happen to be superluminal sources, then one of the expectations is that the X-ray luminosity will be quite variable and the X-ray sources would not necessarily be located near the galaxy nucleus.

6.1.4. *Young X-ray Supernovae*

Although not much is known about how common these objects are, they typically emit with ROSAT X-ray luminosities up to $\sim 10^{40}$ erg s $^{-1}$ (cf. Schlegel 1995). Schlegel, Petre & Colbert (1996) monitored the X-ray bright supernova SN 1978K over a period of ~ 4 years and found it to be constant, even though models (e.g. Chevalier & Fransson 1994) had predicted the light curve to drop in that amount of time. If these objects are indeed common and stay X-ray luminous for long periods of time, then they might be considered possible candidates for the compact X-ray sources we find in our sample of galaxies. They would presumably often be off-nuclear sources since most detected X-ray supernovae are of type II (cf. Schlegel 1995), which would tend to be found in star-forming regions located throughout the galaxy.

6.2. Statistical Results from the HRI Survey

6.2.1. *Sources with Previous Evidence for Nuclear Activity or Central Black Holes*

Several of the elliptical galaxies in the sample are also radio galaxies with large-scale jets, indicating the presence of an AGN. The galaxies of this type are NGC 4278 (Wrobel & Heeschen 1984), NGC 4374 (M84; Bridle & Perley 1984), and NGC 4552 (Wrobel & Heeschen 1984). We find compact X-ray sources in HRI images of all three of these galaxies.

Of the 39 galaxies in our sample, four galaxies (NGC 221 [M32], NGC 4278, NGC 4374

[M84], and NGC 4552 [M89]) have previous evidence for a central dark core of mass $10^{6.5}$, $10^{9.2}$, $10^{9.2}$, and $10^{8.7}$ M_{\odot} , respectively, from dynamical modelling of the gas or stars in the nuclear region. It is noteworthy that in all four of these galaxies, we found compact X-ray sources, which is highly suggestive that the X-ray emission from the sources in these galaxies comes from accretion onto a central supermassive BH. In three of these four galaxies, the compact X-ray source is coincident (offset $< 10''$) with the galaxy nuclei.

Thirteen of the 39 galaxies in our sample overlap with the large sample of nearby galaxies studied by HFS95. Six of these galaxies have been classified by these authors as having Seyfert-like, LINER-like or “transition” (between LINER and H II region nuclei) nuclear optical spectra (see Table 11). Of these six galaxies, in all but one (NGC 4138, classified S1.9) galaxy, we found a compact X-ray source. In addition, in all five of these galaxies, the compact X-ray source is coincident with the galaxy nuclei.

EDITOR: PLACE TABLE 11 HERE.

This evidence together suggests that many of the compact X-ray sources in our sample are caused by accretion processes onto supermassive BHs, similar to the processes involved in AGNs. However, as noted by Petre et al. (1993), in the LINER galaxy M81 there is no evidence for an accretion disk. This may also be the case for the other AGN-like sources in our sample. Since ADAF models do not involve thin accretion disks, they make an obvious choice for the physical process involved in explaining the X-ray emission from these AGN-like compact X-ray sources in our sample.

6.2.2. Sources with No Previous Evidence for Nuclear Activity

Of the remaining 33 galaxies *not* known to have Seyfert-like or LINER-like optical nuclear spectra, we find compact near-nuclear X-ray sources in nearly half (15) of them. It is these 33 galaxies that make up a sample of truly “normal” galaxies and our detection frequency of $\sim 50\%$ indicates that luminous compact X-ray sources are quite common in normal galaxies.

Note that of the 9 galaxies with offsets $>10''$, all are classified as either H II region galaxies or are unclassified or normal galaxies (i.e., none are classified as having Seyfert-like or LINER-like nuclei).

There are 16 galaxies with normal (or H II region) nuclei in which we find compact X-ray sources. Nine (56%) of these 16 sources are located $>10''$ from the galaxy nucleus, a far greater percentage than for the AGN-like galaxies (0%; 0 of 5 galaxies).

One might first suggest that many of these sources are merely X-ray binaries that are located near the galaxy nucleus, as has been argued for M32 (Loewenstein et al. 1998) and M33 (Dubus et al. 1997). The X-ray luminosities of the normal galaxy sources are significantly lower than for the AGN-like sources (mean luminosity 2.4×10^{39} erg s $^{-1}$ *vs.* 4.4×10^{39} erg s $^{-1}$), also suggestive that there are two different classes of sources.

As discussed in section 4.5, we found no noticeable difference in luminosity between X-ray sources with large offsets and those with small offsets. However, as can be seen in Figure 4, those galaxies with previous evidence for nuclear activity (filled rectangles) have smaller separations and higher luminosities.

6.2.3. Other Properties

There does not seem to be any correlation between the size of the galaxy (e.g., dwarf or normal-size galaxy) and the offset of the central X-ray source. We also note that the presence of H II regions in the nuclei of the galaxies does not seem to be correlated with the offset of the X-ray sources.

6.3. The L_X vs. L_B Relationship

As discussed by Canizares, Fabbiano & Trinchieri (1987), discrete X-ray sources in external galaxies may make a significant contribution to their total X-ray luminosity. These authors find a simple relationship between the blue luminosity from stars and the predicted X-ray emission from X-ray binaries. In Figure 5, we show a plot of the ROSAT 0.2–2.4 keV luminosities of nuclear pointlike sources in the elliptical, spiral, irregular and dwarf galaxies in our sample and compare it to the predicted X-ray luminosities from X-ray binaries from the Canizares et al. relationship. The blue luminosities for the galaxies have been corrected to the 15" radius aperture used for the X-ray luminosities, using the blue fluxes in Table 1 and the correction factors listed in Table 5. We used the digital sky B-band survey plates to estimate these correction factors. We should note that the relationship between L_X and L_B used by Canizares et al. is based on the observed luminosities of globular clusters and of sources in the bulge of M31. We have included a correction from the 0.5–4.5 keV band to the 0.2–2.4 keV band assuming a power-law spectrum with photon index $\Gamma = 1.7$.

Note that all of the galaxies in our sample have X-ray luminosities in excess (by up to three orders of magnitude) of that predicted for X-ray binaries. The conclusion is that, in this 15" radius region, the X-ray to blue luminosity ratio is up to 10^3 times larger than that found for normal galaxies (Canizares et al. 1987). It is highly suggestive that

the X-ray emission is not from normal X-ray binaries, but is from other sources, such as superluminous X-ray binaries, low-luminosity AGN or X-ray bright supernovae.

EDITOR: PLACE FIGURE 5 HERE.

6.4. Nature of the Elliptical Galaxy X-ray Sources

There are four elliptical galaxies in our sample (NGC 4278, NGC 4374, NGC 4406 and NGC 4552). We have chosen to discuss the results from these galaxies separately since it is known that these galaxies have extended emission from hot gas (Forman et al. 1985) as well as other components, such as the compact nuclear X-ray sources under study. Matsushita et al. (1994) discovered a hard X-ray component in ASCA spectra of five early-type galaxies in addition to the hot gas component dominating at soft ($\lesssim 2$ keV) energies. As noted by Matsumoto et al. (1997), the X-ray luminosity of the hard component in a sample of 12 early-type galaxies exceeds that predicted for the discrete X-ray binary population (as estimated from the blue luminosity, Canizares et al. 1987) for three of the 12 galaxies. Matsumoto et al. explain this excess as probably due to X-ray emission from AGNs in these galaxies.

Referring back to Figure 5, we note that all of the elliptical galaxies in our sample have ROSAT luminosities (corresponding with the “nuclear” source) in excess of that predicted by an X-ray binary component. This excess could be a hard component from an AGN, or a soft thermal component localized within the HRI point-spread function.

The three elliptical galaxies NGC 4374, NGC 4406 and NGC 4552 have extended thermal emission within the 15'' radius used to extract counts for the quoted ROSAT luminosity. Using the correction factors for the point-like component from section 3.1, we

compared the point-like component of the 0.2–2.4 keV ROSAT count rate to that predicted from the hard (power-law) component of the ASCA model (which includes flux from a much larger region). Note that in none of these three objects is the hard component resolved by ASCA. The hard (power-law) component was a factor of 3.1, 12.5 and 1.2 times larger than the ROSAT point-like component (for galaxies NGC 4374, NGC 4406 and NGC 4552, respectively). This indicates that the hard component may be extended in some cases (e.g. Matsushita et al. 1994). Another possibility is that the hard (or point-like) component varied in intensity between the ROSAT HRI and ASCA observations.

We next turn to the results from the ASCA spectral fitting of the elliptical galaxies NGC 4374, NGC 4406 and NGC 4552. Two (NGC 4374 and NGC 4552) galaxies are also radio galaxies and have dynamical evidence for a central dark core of mass $\sim 10^9 M_\odot$. The best fit model for these three sources was a Raymond-Smith plasma plus a power-law model, with the power-law slopes $\Gamma \sim 2.0$ –3.4 and thermal plasma temperatures 0.7–0.8 keV. Note that these three galaxies are in dense environs. The temperatures are consistent with hot gas known to be present in elliptical galaxies, but the power-law slopes, if from AGN with $M(BH) \sim 10^9 M_\odot$, imply a different accretion process than typical Seyfert 1 galaxies, since their slopes are steeper than those seen in Seyferts by $\gtrsim 1$.

The unabsorbed X-ray luminosities of the hard power-law components are $\sim 2 \times 10^{40}$ erg s^{−1} in the 2–10 keV band, for each of the three elliptical galaxies (see Table 12). This is again different (much lower) than what is found for typical Seyfert galaxies. Using the dynamical BH masses of $\sim 10^9 M_\odot$ (Table 11) and assuming $L_X(2$ –10 keV) $\sim 0.1 L_{Bol}$ (e.g., Elvis et al. 1994), this implies $L/L_{Edd} \lesssim 10^{-6}$, which is much lower than estimated values of L/L_{Edd} for classical AGN (cf. Wandel 1991).

EDITOR: PLACE TABLE 12 HERE.

Matsushita et al. (1994) ascribe the hard X-ray emission in elliptical galaxy spectra to discrete X-ray sources in the galaxy or to foreground/background emission from the hot intracluster medium of the Virgo cluster. We find that the hard X-ray emission has a spectral slope consistent with XRBs in their soft state and could indeed be emission from ~ 100 XRB (assumed to be emitting at their Eddington limit). However, another interpretation is that the central dark core is a black hole, and an AGN accretes gas via an accretion disk and produces $\sim 2 \times 10^{40}$ erg s $^{-1}$ of X-ray emission. This interpretation is further supported by the high L_X/L_B ratio for these elliptical galaxies (section 6.3). As mentioned previously, narrow-line Seyfert 1 galaxies are an example of AGN with such steep ($\Gamma \approx 2.5$) spectra slopes. This interpretation is supported by the fact that, as mentioned earlier, two of the three galaxies have central dark cores with masses $\sim 10^9$ M $_{\odot}$.

Note that the RS+PL models for the elliptical galaxies yield absorbing column in the range $3.5\text{--}7.7 \times 10^{21}$ cm $^{-2}$. These values are slightly lower than those found in Seyfert 2 galaxies (e.g., mean values of $\sim 10^{22}\text{--}10^{23}$ cm $^{-2}$, Turner et al. 1997), which are thought to be due to absorbing tori viewed edge-on.

6.5. Nature of the Spiral Galaxy X-ray Sources

Two (NGC 1313 and NGC 5408) of the three spiral galaxies in our ASCA sample have central X-ray sources that are offset ~ 1 kpc from the photometric center of the galaxy. In the third galaxy (M33), the central X-ray source is only offset by ~ 9 pc (2.6" – not significantly different from zero). Such large separations might be considered unfeasible if the X-ray sources were supermassive BHs (e.g. with masses $\gtrsim 10^6$ M $_{\odot}$). However, if the objects have masses $\lesssim 10^3$ M $_{\odot}$, the mass of the objects is only a small fraction of the dynamical mass in the central kpc (which may be $\sim 10^7\text{--}10^8$ M $_{\odot}$). So, it is not infeasible that an object of mass $\lesssim 10^3$ M $_{\odot}$ be found ~ 1 kpc from the photometric (assumed

dynamical) center of the galaxy.

A list of the 2–10 keV unabsorbed luminosities of the X-ray sources in the three spiral galaxies is given in Table 11 (as predicted by the DBB+PL model). The masses predicted by the BM model imply Eddington ratios of ~ 0.04 for M33 and NGC 1313, but a slightly smaller Eddington ratio of 0.002 for NGC 5408. These Eddington ratios are significantly larger than that estimated for the ADAF LINER galaxy NGC 4258 ($\sim 10^{-4}$, Lasota et al. 1996).

The X-ray sources in the spiral galaxies have 2–10 keV X-ray luminosities $\sim 0.6\text{--}3 \times 10^{39}$ erg s $^{-1}$, which are an order of magnitude smaller than the hard components in the elliptical galaxies, indicating that they may be of different origin. These luminosities are still one or two orders of magnitude brighter than typical BH binaries (e.g. Tanaka & Lewin 1995), which are thought to have BHs of masses on the order of a few solar masses. If we roughly scale the masses to the X-ray luminosities ($M_{BH} \sim 10^6\text{--}10^9 M_\odot$ for $L_X \sim 10^{42}\text{--}10^{44}$ erg s $^{-1}$), we arrive at masses consistent with those predicted by the BM model ($\sim 10^2 - 10^6 M_\odot$).

Values of $r_{in}(\cos \theta)^{\frac{1}{2}}$ and kT_{in} for LMXBs are typically 5–10 km and 1.0–1.5 keV, respectively, whereas for BHCs, the values are 20–30 km and 0.6–1.0 keV, respectively (e.g., see Yaqoob, Ebisawa, & Mitsuda 1993). As mentioned in section 5, for M33 and NGC 1313#2, the values of $r_{in}(\cos \theta)^{\frac{1}{2}}$ are much higher than typical values for LMXBs and are more consistent with the range for BHCs. However, kT_{in} is more consistent with the range for the LMXBs. We disregard the fitting results from NGC 1313#1, since its shallow slope suggests it is not in a soft (high) state. The results for NGC 5408 are indeed much different than might be expected for a LMXB or “normal” BHC. The value of $r_{in}(\cos \theta)^{\frac{1}{2}}$ is very high (2200 – 62500 km) and kT_{in} is much lower than expected for a “normal” BHC.

We should note that in the standard thin accretion disk theory, r_{in} extends inward to

the radius of the innermost stable orbit, which is equal to $3r_g$ for a Schwarzschild BH. In Table 9, we list the corresponding BH mass for $r_{in}(\cos\theta)^{\frac{1}{2}} = 3r_g$. Note that these masses are much lower than those predicted by the BM model. The discrepancy can be explained by the fact that the multicolor disk blackbody model used by XSPEC approximates $T(r) \propto r^{-3/4} (1 - (6r_g/r)^{\frac{1}{2}})$ as $T(r) \propto r^{-3/4}$, so it underpredicts the normalization and thus also the value of $r_{in}(\cos\theta)^{\frac{1}{2}}$ (L. Titarchuk, priv. comm.). Therefore, values of $r_{in}(\cos\theta)^{\frac{1}{2}}$ are only useful for relative comparisons (e.g., to values predicted for other objects), but not for estimates of the innermost stable orbit and thus the mass of the BH.

It is noteworthy, however, that the predicted mass of the X-ray emitting BH in NGC 5408 (from the BM model) is $\sim 10^2$ – 10^3 times as large as that for M33 or NGC 1313, so it is consistent that NGC 5408 is a BHC with a larger BH mass.

So, the working model is that these X-ray objects are BH candidates of mass $\sim 10^2$ – $10^4 M_\odot$, currently in their soft (high) state (except for the observation NGC 1313#1, which is consistent with a BHC in its hard state).

It is not clear how BHs of mass $\sim 10^2$ – $10^4 M_\odot$ would form. Brown & Bethe (1994) indicated that there are two types of BHs that are formed at the end of stellar evolution: $\sim 1.5 M_\odot$ BHs from supernova explosions of massive main sequence stars, and $\sim 10 M_\odot$ BHs from the collapse of the helium core of stars more massive than 25 – $30 M_\odot$. The masses implied for M33, NGC 1313 and NGC 5408 are much higher than can be explained by either of these processes.

At the other extreme are supermassive BHs which are present in the nuclei of AGNs (and possibly in the nuclei of other “inactive” galaxies as well). These BHs are assumed to be formed by the collapse of primordial gas clouds (e.g., Silk & Rees 1998), but formation of BHs with masses $\lesssim 10^6 M_\odot$ are noted to be less efficient and the production of such BHs is likely to be inhibited. One reason why such objects are prevented from forming is that

primordial clouds of mass $\lesssim 10^9 M_\odot$ are readily disrupted by supernova-driven winds (Dekel & Silk 1986). Therefore, the BH masses of the X-ray sources described in this paper are not likely to have been formed by collapse of a primordial cloud.

Lee (1995) offers a possible explanation for intermediate-mass BHs, in which stellar-size BHs ($M \lesssim 10 M_\odot$) merge and can form a seed BH of mass $\sim 100 M_\odot$.

We find that the DBB+PL model predicts intrinsic absorbing columns of $\sim 1-3 \times 10^{21} \text{ cm}^{-2}$. These columns are not typical of the large columns through absorbing tori in Seyfert 2 galaxies. This implies, that if the objects do have surrounding optically-thick tori like those found in AGNs, then either the line-of-sight through the tori is not edge-on, or the tori are not as optically thick as those in AGNs.

6.6. The Nature of the Compact X-ray Sources

There does not seem to be a single explanation that works for all of the compact X-ray sources. For example, the X-ray luminosities of the sources in the galaxies with previous evidence for nuclear activity are significantly larger than those luminosities of the sources in the otherwise normal galaxies. The mean separation of the X-ray sources from the galaxy nucleus is also larger for the normal galaxies. This suggests that there may be two different types of X-ray emitting objects in these two types of galaxies.

The soft components in the ASCA spectra in the elliptical galaxies are better fit by a Raymond-Smith thermal plasma than a multicolor disk blackbody model. This suggests that some of the X-ray emission from the central X-ray sources in the elliptical galaxies may be emission from hot gas, a component which has been known to be present in many other elliptical galaxies (Forman et al. 1985).

What does seem to be universal among the X-ray sources is that they have relatively

steep spectral slopes compare with those of Seyfert 1 nuclei. This, and the fact that large absorbing columns are not found, suggests that the X-ray sources are probably different physically or geometrically from typical AGN in active X-ray bright galaxies.

We should also mention that the preference for low absorbing columns could also be due to a selection effect. X-ray sources with similar intrinsic (unabsorbed) luminosities but larger absorbing columns (e.g., $N_H \sim 10^{23} - 10^{24} \text{ cm}^{-2}$) would be considerably weaker ROSAT X-ray sources.

7. Summary and Conclusions

Using archival ROSAT HRI observations, we have used a distance-limited sample of 39 nearby galaxies to search for compact “nuclear” X-ray sources. We found compact X-ray sources within $\sim 2'$ of the nucleus (photometric center) of 21 of the 39 galaxies. Approximately 40% (9 of 21) of the compact X-ray sources were located $> 10''$ ($\gtrsim 0.3 \text{ kpc}$ at the mean distance of our sample) from the photometric center of the galaxy.

Compact X-ray sources are found in nearly all cases in which previous possible evidence for a BH or an AGN had been found (e.g., large-scale radio sources, dynamical dark core masses $> 10^6 M_\odot$, or optical spectral classification as Seyfert, LINER, or “transition” object). This indicates that some of the X-ray sources in these galaxies are probably AGN or at least accretion-driven objects with supermassive BHs.

We analyzed archival ASCA spectra of six of the 21 galaxies with compact X-ray sources (3 spiral galaxies and 3 elliptical galaxies). The elliptical galaxy spectra are adequately fit with a two-component Raymond-Smith thermal plasma model plus an absorbed power-law model. The intrinsic absorption of the power-law source was typically several $\times 10^{21} \text{ cm}^{-2}$ (significantly smaller than seen in Seyfert 2 galaxies) and the power-law

slope was significantly steeper ($\Gamma \approx 2.5$) than seen in type 1 or 2 AGNs. The spiral galaxy spectra are well-fit by a two-component model consisting of a multicolor disk blackbody model plus a power-law model. Assuming both components suffer the same intrinsic absorption, we find intrinsic absorption of a few 10^{21} cm^{-2} and, again, steep power-law slopes of $\Gamma \approx 2.5$. The central X-ray source in the spiral galaxy NGC 1313 seems to have changed from a hard state to a soft state in the 2.4 intervening years between observations. The spiral galaxy X-ray sources, when fit with the Bulk Motion Comptonization model of Shrader & Titarchuk (1998), predict black hole masses $\sim 10^2 - 10^4 \text{ M}_\odot$. This model assumes the presence of a thin disk surrounding the black hole.

The emerging picture of the compact X-ray sources in nearby galaxies is that they are probably high-mass ($M \gtrsim 10 \text{ M}_\odot$) accreting black holes. It is not clear whether they are binary systems or not, but the steep hard X-ray emission is consistent with that of a BHC in its soft (high) state. Such steep slopes are also consistent with what has been observed in Narrow-Line Seyfert 1 galaxies.

The X-ray sources in the spiral galaxies seem to have BHs of intermediate mass ($\sim 10^2 - 10^4 \text{ M}_\odot$), which make them members of a unique class of accreting black holes. BHs of this mass range are not predicted in most theories of BH formation. Except for the central X-ray source in M33, there are not any such objects in the Local Group (M31, the Milky Way, SMC, LMC) that are known to emit at intermediate X-ray luminosities of $L_X \sim 10^{39} - 10^{40} \text{ erg s}^{-1}$. Future studies of these interesting objects in nearby galaxies are imperative for determining their exact nature.

EJMC would like to thank Lev Titarchuk for many helpful discussions and for calculations having to do with the bulk motion model. EJMC acknowledges support from the National Research Council. This research has made extensive use of the NASA/IPAC Extragalactic Database (NED), which is operated by the Jet Propulsion Laboratory,

Caltech, under contract with NASA. The Digital Sky Survey data were retrieved from the STScI WWW page and were produced under US government grant NAGW-2166.

Table 1. Sample of Nearby Galaxies

Galaxy Name	Other Name	R.A. ^a (J2000)	Dec. ^a	cz ^a (km s ⁻¹)	D ^b (Mpc)	ref. ^b	Gal. Type ^a	Log Axial Ratio ^a	f _B ^c (log erg s ⁻¹ cm ⁻²)	f _{FIR} ^d (log erg s ⁻¹ cm ⁻²)
NGC 205	M110	0 40 22.5	+41 41 11	-232	0.7	1	-5.0	0.30	-8.70	-10.17
NGC 221	M32	0 42 41.9	+40 51 55	-205	0.7	1	-6.0	0.13	-8.68	...
NGC 300		0 54 53.8	-37 40 57	142	1.2	1	7.0	0.15	-8.58	-8.77
NGC 598	M33	1 33 50.9	+30 39 37	-179	0.7	1	6.0	0.23	-7.49	< -9.04
NGC 1313		3 18 15.5	-66 29 51	457	3.7	1	7.0	0.12	-8.90	-9.03
NGC 1396		3 38 06.3	-35 26 25	894	16.9	2	-3.0	0.07	-11.10	...
AM 0337-353		3 39 13.6	-35 22 19	952	16.9	2	-2.0	0.10	-11.30	...
IC 342		3 46 49.7	+68 5 45	34	3.9	1	6.0	0.01	-7.42	-8.36
NGC 1705		4 54 13.6	-53 21 44	673	6.0	1	-3.0	0.13	-10.22	-10.29
NGC 2403		7 36 54.5	+65 35 58	131	4.2	1	6.0	0.25	-8.56	-8.85
Ho II		8 19 06.0	+70 42 51	158	1.4	3	10.0	0.10	-9.54	-10.15
ESO 495-G21	He 2-10	8 36 15.0	-26 24 34	896	6	4	90.0	0.11
UGC 5086		9 32 54	+21 29 0	448	2	5	10.0	0.00
NGC 3031	M81	9 55 33.5	+69 4 00	-34	1.4	1	2.0	0.28	-8.14	-9.20
Ho IX		9 57 30	+69 2 0	46	1.4	3	10.0	0.09	-10.82	...
Leo A		9 59 18	+30 44 0	20	6	5	10.0	0.22	-10.26	...
NGC 3990		11 57 36.3	+55 27 33	696	17.0	1	-3.0	0.24	-10.57	...
NGC 4138		12 9 30.8	+43 41 16	923	17.0	1	-1.0	0.18	-10.03	...
NGC 4150		12 10 33.5	+30 24 06	244	9.7	1	-2.0	0.16	-10.15	-10.16
NGC 4190		12 13 44.7	+36 38 00	230	2.8	1	10.0	0.04	-10.53	-10.57
UGCA 276	DDO 113	12 14 54	+36 13 0	284	4	5	10.0	0.00
UGC 7356		12 19 0	+47 5 0	272	4	5	10.0	0.03
NGC 4278		12 20 07.2	+29 16 47	649	9.7	1	-5.0	0.03	-9.58	-10.42
NGC 4286		12 20 41.8	+29 20 38	623	10	6	0.0	0.20	-10.74	...

Table 1—Continued

Galaxy	Other	R.A. ^a	Dec. ^a	<i>cz</i> ^a	D ^b	ref. ^b	Gal.	Log	f _B ^c	f _{FIR} ^d
Name	Name	(J2000)		(km s ⁻¹)	(Mpc)	Type ^a	Axial	(log erg s ⁻¹ cm ⁻²)	(log erg s ⁻¹ cm ⁻²)	
NGC 4374	M84	12 25 03.7	+12 53 15	910	16.8	1	-5.0	0.06	-9.19	-10.54
IC 3303		12 25 15.0	+12 42 53	-213	16.8	7	-4.4	0.20	-11.06	...
NGC 4387		12 25 41.8	+12 48 42	561	16.8	1	-5.0	0.21	-10.34	...
NGC 4406	M86	12 26 11.8	+12 56 49	-248	16.8	1	-5.0	0.19	-9.08	...
NGC 4449		12 28 11.4	+44 5 40	201	3.0	1	10.0	0.15	-9.16	...
NGC 4485		12 30 31.7	+41 42 01	493	9.3	1	10.0	0.15	-10.08	...
IC 3540		12 35 27.3	+12 45 00	733	16.8	7	11.0	0.10	-11.12	...
NGC 4552	M89	12 35 39.9	+12 33 25	311	16.8	1	-5.0	0.04	-9.42	...
NGC 4569	M90	12 36 50.1	+13 9 48	-235	16.8	1	2.0	0.34	-9.10	-9.26
NGC 4627		12 41 59.7	+32 34 29	765	7.5	8	-5.0	0.16	-10.38	...
NGC 5204		13 29 36.4	+58 25 04	204	4.8	1	9.0	0.22	-9.78	-9.84
NGC 5408		14 4 22	-41 22 18	509	4.9	1	9.7	0.31	-9.86	-9.89
NGC 6822		19 44 57.9	-14 48 11	-56	0.7	1	10.0	0.06	-8.54	-9.40
NGC 6946		20 34 52.0	+60 9 15	52	5.5	1	6.0	0.07	-8.30	-8.42
NGC 7320		22 36 04.2	+33 56 52	776	13.8	1	7.0	0.29	-10.22	...

^aRight ascension, declination, recessional velocity, galaxy type, and axial ratio were taken from RC3.

^bDistance to galaxy and reference. References: (1) Tully 1988; (2) in Fornax cluster, assumed to be at distance of Fornax cluster (16.9 Mpc, Tully 1988); (3) in M81 group, assumed to be at distance of M81 (1.4 Mpc, Tully 1988); (4) Johansson 1987; (5) Melisse & Israel 1994; (6) Sandage & Hoffman 1991; (7) in Virgo cluster, assumed to be at distance of Virgo cluster (16.8 Mpc, Tully 1988); (8) companion to NGC 4631, assumed to be at the distance to NGC 4631 (7.5 Mpc, Hummel et al. 1984)

^cB-band optical flux, calculated from B₀^T (from RC3)

^dFar-infrared flux calculated using the method of Fullmer & Lonsdale 1989, using IRAS fluxes from Moshir et al. 1990 (as listed in the NASA Extragalactic Database [NED])

Table 2. ROSAT Observation Log

Galaxy Name	Seq. No. ^a	Exp. Time ^b (ks)	Galaxy Name	Seq. No. ^a	Exp. Time ^b (ks)
NGC 205	rh600816n00	28.1	UGCA 276	rh600741n00	42.6
NGC 221	rh600600n00	12.7	UGC 7356	rh701008n00	27.6
NGC 300	rh600621a01	19.1	NGC 4278	rh701004a01	5.9
NGC 598	rh400460a01	41.0	NGC 4286	rh701004a01	5.9
NGC 1313	rh500403a01	31.4	NGC 4374	rh600493n00	26.5
NGC 1396	rh600831n00	73.5	IC 3303	rh600493n00	26.5
AM 0337-353	rh600831n00	73.5	NGC 4387	rh600493n00	26.5
IC 342	rh600022n00	19.1	NGC 4406	rh600463a02	10.5
NGC 1705	rh600604n00	26.2	NGC 4449	rh600743n00	15.4
NGC 2403	rh600767n00	26.5	NGC 4485	rh600697n00	6.7
Ho II	rh600745n00	7.8	IC 3540	rh600491a01	30.1
ESO 495-G21	rh600700n00	20.3	NGC 4552	rh600491a01	30.1
UGC 5086	rh600602n00	13.6	NGC 4569	rh600603a01	21.9
NGC 3031	rh600247n00	26.6	NGC 4627	rh600193a01	14.3
Ho IX	rh600247n00	26.6	NGC 5204	rh702723n00	14.9
Leo A	rh600117n00	19.1	NGC 5408	rh600376n00	12.6
NGC 3990	rh600430n00	13.6	NGC 6822	rh600815a01	52.9
NGC 4138	rh701943n00	5.8	NGC 6946	rh600501n00	60.3
NGC 4150	rh600762a01	10.5	NGC 7320	rh800689n00	23.3
NGC 4190	rh600733n00	3.5			

^aROSAT HRI sequence number for archival data

^bExposure time in kiloseconds (Keyword EXPTIME in the FITS headers for the data)

Table 3. ASCA Observations of Nearby Galaxies

Galaxy Name	Seq. No.	Obs. Date (YYYYMMDD)	CCD mode	SIS0 cnt. rate ^a (cnt s ⁻¹)	SIS0 on-time ksec	GIS2 on-time ksec
M33 (#1)	60036000	19930722–19930723	4	0.45	13.8	17.6
M33 (#2)	60036010	19930723	4	0.46	12.9	18.3
NGC 1313 (#1)	60028000	19930712–19930713	4	0.066	18.2	29.8
NGC 1313 (#2)	93010000	19951129–19951130	1	0.051	30.4	36.3
NGC 4374	60007000	19930704	2	0.071	14.0	21.1
NGC 4406	60006000	19930703–19930704	2	0.29	5.7	20.9
NGC 4552	63023000	19950626–19950627	2	0.032	27.6	27.8
NGC 5408	930111000	19950208–19950209	2	0.048	44.6	48.5

^aCount rate in the SIS0 detector for the energy range 0.4–10 keV

Table 4. Galaxies without Detected Nuclear X-ray Sources

Galaxy Name	Cnt Rate ^a 10^{-2} s^{-1}	$N_H^{Gal,b}$ 10^{20} cm^{-2}	f_X 10^{-13} cgs	L_X 10^{38} cgs
NGC 205	< 0.47	6.75	< 2.633	< 0.154
NGC 300	< 0.24	3.23	< 1.119	< 0.193
NGC 1396	< 0.41	1.35	< 1.573	< 53.8
AM 0337-353	< 0.31	1.30	< 1.180	< 40.3
NGC 1705	< 0.36	4.19	< 1.787	< 7.70
UGC 5086	< 0.24	3.08	< 1.106	< 0.529
Ho IX	< 0.31	4.07	< 1.528	< 0.358
Leo A	< 0.32	1.68	< 1.285	< 5.54
NGC 3990	< 0.24	1.21	< 0.9010	< 31.2
NGC 4138	< 0.68	1.36	< 2.613	< 90.4
UGCA 276	< 0.33	1.49	< 1.292	< 2.47
UGC 7356	< 0.31	1.16	< 1.154	< 2.21
NGC 4286	< 0.15	1.79	< 0.6106	< 7.31
IC 3303	< 0.43	2.58	< 1.901	< 64.2
NGC 4387	< 0.30	2.60	< 1.329	< 44.9
IC 3540	< 0.27	2.55	< 1.191	< 40.2
NGC 4627	< 0.27	1.27	< 1.023	< 6.89
NGC 7320	< 0.26	7.96	< 0.9878	< 22.5

^a3 σ upper limit to the count rate for a 15" radius circle detect cell^bGalactic absorbing column calculated with HEASARC's on-line Galactic hydrogen database (data from Dickey & Lockman 1990)

Table 5. Compact X-ray Sources in Nuclear Regions of Nearby Galaxies

Galaxy Name	X-ray Position (J2000)		Offset ^b (arcsec)	Cnt Rate ^c 10^{-2} s^{-1}	$N_H^{Gal,d}$ 10^{20} cm^{-2}	f_X^e 10^{-13} cgs	L_X^e $10^{38} \text{ erg s}^{-1}$	$\log(f_B)^f$
	R.A. ^a	Dec. ^a	(pc)					
M32	00 42 42.7	+40 51 51.1	9.9	33.6	1.19	6.34	6.556	0.384
M33	01 33 51.1	+30 39 37.0	2.6	8.8	7.23 ^g	5.58	38.53 ^g	2.26 ^g
NGC 1313	03 18 20.3	−66 29 11.3	49.0	879	3.01	3.90	14.68	24.1
IC 342	03 46 48.6	+68 05 51.0	8.6	163	0.65	30.2	6.603	12.0
NGC 2403	07 36 55.7	+65 35 42.6	17.1	348	0.36	4.11	1.779	3.76
Ho II	08 19 29.7	+70 42 18.4	121.9	827	11.99	3.42	56.65	13.3
ESO 495-G21	08 36 15.3	−26 24 32.7	4.2	122	0.47	9.84	2.928	38.6
M81	09 55 33.4	+69 03 53.1	6.9	46.8	11.99 ^g	4.16	5.940 ^g	1.39 ^g
NGC 4150	12 10 34.7	+30 24 00.9	16.3	767	2.23	1.62	8.886	100.0
NGC 4190	12 13 45.3	+36 37 58.5	7.4	100	2.35	1.54	9.266	8.69
NGC 4278	12 20 06.7	+29 16 50.4	7.4	348	1.72	1.77	6.987	78.7
NGC 4374	12 25 03.7	+12 53 13.5	1.5	122	0.29 ^g	2.60	1.278 ^g	43.2 ^g
NGC 4406	12 26 11.7	+12 56 46.7	2.7	220	0.30 ^g	2.62	1.339 ^g	45.3 ^g
NGC 4449	12 28 09.4	+44 05 07.1	39.3	572	0.57	1.37	1.940	2.09
NGC 4485	12 30 30.5	+41 41 45.5	20.5	924	0.39	1.78	1.586	16.4
NGC 4552	12 35 39.7	+12 33 28.6	4.6	375	0.28 ^g	2.57	1.232 ^g	41.6 ^g
NGC 4569	12 36 49.7	+13 09 47.2	5.9	481	0.46	2.49	1.654	55.9
NGC 5204	13 29 38.6	+58 25 03.2	17.3	403	2.50	1.39	9.649	26.6
NGC 5408	14 03 19.4	−41 22 57.7	49.3	1171	4.88	5.66	26.11	75.0
NGC 6822	19 44 56.4	−14 48 29.3	28.4	96.4	0.35	9.49	1.334	0.0782
NGC 6946	20 34 52.4	+60 09 09.9	5.9	157	0.24	21.1	2.003	7.25

^aX-ray position of compact source. The uncertainties in the X-ray positions are $\sim 10''$ due to pointing uncertainties of the ROSAT spacecraft.

^bOffset of X-ray position from optical photometric center (Table 1)

^cHRI count rate using source region of 15'' radius circle

^dGalactic absorption column (Dickey & Lockman 1990)

^e0.2–2.4 keV X-ray flux (units $\text{erg s}^{-1} \text{ cm}^{-2}$) and luminosity, assuming a power-law spectrum (see text) and absorption column listed in the Table. Distances listed in Table 1 were used to compute luminosities.

^fLogarithm of the fraction of blue light in the 15'' radius aperture centered on the X-ray position (columns 2 and 3) compared with the blue light from the whole galaxy. See section 6.3.

^gHRI count rates, fluxes and luminosities have been corrected to reflect the contribution from the point-like component (see section 3.1)

Table 6. Single-Component Fits to ASCA Data

Galaxy Name	Model ^a	Γ or kT (keV) ^b	Normalization ^c	N_H ^d (10^{21} cm $^{-2}$)	Abundance ^e	χ^2 / d.o.f. ^f
Spiral Galaxies						
M33 (#1)	PL	$\Gamma = 2.33$ $2.28 - 2.37$	6.95×10^{-3}	3.20 2.94 – 3.47		659 / 595
	RS	$kT = 3.33$ $3.17 - 3.48$	1.88×10^{-2}	1.45 1.28 – 1.64	0 < 0.05	555 / 594
M33 (#2)	PL	$\Gamma = 2.31$ $2.27 - 2.35$	7.42×10^{-3}	2.99 2.77 – 3.21		838 / 676
	RS	$kT = 3.43$ $3.31 - 3.56$	2.00×10^{-2}	1.27 1.14 – 1.41	0 < 0.04	652 / 675
NGC 1313 (#1)	PL	$\Gamma = 1.74$ $1.67 - 1.82$	4.74×10^{-4}	0.151 < 0.57		244 / 259
	RS	$kT = 6.68$ $5.92 - 7.47$	1.77×10^{-3}	0 < 0.09	0.10 < 0.27	253 / 258
NGC 1313 (#2)	PL	$\Gamma = 2.77$ $2.65 - 2.88$	1.27×10^{-3}	2.95 2.50 – 3.43		185 / 198
	RS	$kT = 2.05$ $1.87 - 2.24$	3.16×10^{-3}	0.910 0.596 – 1.23	0.06 < 0.14	196 / 197
NGC 5408	PL	$\Gamma = 2.39$ $2.33 - 2.48$	4.20×10^{-4}	0 < 0.29		261 / 269
	RS	$kT = 2.02$ $1.86 - 2.19$	1.64×10^{-3}	0 < 0.04	0.03 < 0.12	343 / 268

Table 6—Continued

Galaxy Name	Model ^a	Γ or kT (keV) ^b	Normalization ^c	N_H ^d (10^{21} cm $^{-2}$)	Abundance ^e	χ^2 / d.o.f. ^f
Elliptical Galaxies						
NGC 4374	PL	$\Gamma = 3.29^g$	1.13×10^{-3}	1.69 ^g		447 / 216
	RS	$kT = 0.79$	4.94×10^{-3}	1.10	0.08	372 / 215
		$0.75 - 0.82$		$0.71 - 1.59$	$0.06 - 0.11$	
NGC 4406	PL	$\Gamma = 5.72^g$	9.42×10^{-3}	5.15 ^g		1189 / 386
	RS	$kT = 0.80$	6.69×10^{-3}	1.41	0.40	459 / 385
		$0.77 - 0.82$		$0.86 - 2.10$	$0.31 - 0.57$	
NGC 4552	PL	$\Gamma = 2.24$	2.70×10^{-4}	0.558		404 / 248
		$2.06 - 2.44$		$0.088 - 1.07$		
	RS	$kT = 0.76$	2.11×10^{-3}	2.23	0.10	454 / 247
		$0.71 - 0.81$		$1.45 - 3.35$	$0.07 - 0.16$	

NOTE: Ranges for parameters are given for 90% confidence for one interesting parameter ($\Delta\chi^2 = 2.7$).

^aEmission model used in the spectral fit: PL = power-law model and RS = Raymond-Smith thermal plasma model.

^bPhoton spectral index Γ for the power-law model and gas temperature kT for the RS model.

^cNormalization for the PL and RS models. Units for the PL model are photons keV $^{-1}$ cm $^{-2}$ s $^{-1}$ at 1 keV. For the RS model, the normalization is equal to $10^{-14} / (4\pi D^2) \int n_e n_H dV$, where D is the distance to the X-ray source in cm, n_e (n_H) is the electron (hydrogen) density in units of cm $^{-3}$, and V is the volume of the X-ray emitting source.

^dEffective neutral hydrogen absorbing column density.

^eAbundance of metals in the thermal plasma, relative to cosmic abundances.

^f χ^2 value for the fit and number of degrees of freedom (no. spectral bins - no. of fit parameters).

^gFit is too poor to use χ^2 statistics to find error range (i.e., $\chi^2_\nu > 2.0$).

Table 9. Inner Radius of Accretion Disk for Spiral Galaxies

Galaxy Name	kT_{in}^a (keV)	$R_{in} (\cos \theta)^{\frac{1}{2}} a$ (km)	$M(R_{in} (\cos \theta)^{\frac{1}{2}} = 3r_g)^b$ (M_{\odot})	$M(BH)^c$ (M_{\odot})
M33 #1	1.15	37.1 (29.7 – 49.1)	4.2	116.7
M33 #2	1.15	40.8 (34.4 – 50.6)	4.6	117.6
NGC 1313 #2	1.34	33.4 (< 75.8)	3.8	590
NGC 5408	0.13	18090 (2191 – 62559)	2044	$\sim 8-9 \times 10^3$

^aTemperature kT_{in} at the inner radius of the accretion disk (column 1) and the inner radius of accretion disk times the square root of the cosine of the inclination angle (column 2), as given by the normalization of the multicolor disk blackbody model. Ranges are given based on 90% confidence ranges of the normalizations to the DBB+PL fits in Table 6

^bMass of the central black hole if the inner radius $r_{in}(\cos \theta)^{\frac{1}{2}}$ is assumed to be at 3 Schwarzschild radii (the innermost stable circular orbit for a Schwarzschild black hole). Note that this mass is assumed incorrect (see text section 6.3.2)

^cMass of the central black hole, as given by the normalization of the bulk motion model.

Table 10. Bulk Motion Fits to Spiral Galaxy ASCA Spectra

Galaxy Name	kT ^a (keV)	Γ ^b	$\log f$ ^c	Normalization ^d	N_H ^e (10^{21} cm $^{-2}$)	χ^2 / d.o.f. ^f
M33 # 1	0.46 0.45 – 0.47	1.96 1.87 – 2.06	-1.78×10^{-5}	1.58×10^{-4}	0 < 0.026	687 / 593
M33 # 2	0.47 0.46 – 0.48	2.00 1.93 – 2.09	-1×10^{-5}	1.75×10^{-4}	0 < 0.016	873 / 674
NGC 1313 #1	0.12 0.11 – 0.15	1.80 1.72 – 1.86	-1.61×10^{-5}	2.17×10^{-5}	1.39 0.94 – 1.89	238 / 257
NGC 1313 #2	0.33 0.29 – 0.35	2.17 2.03 – 2.33	-3.06×10^{-5}	2.09×10^{-5}	0 < 0.726	194 / 196
NGC 5408	0.12 0.11 – 0.14	2.35 2.22 – 2.45	-2.42×10^{-5}	2.03×10^{-5}	0.60 0.28 – 0.95	256 / 267

NOTE: Ranges for parameters are given for 90% confidence for one interesting parameter ($\Delta\chi^2 = 2.7$).

^aTemperature of the disk for BM model.

^bPhoton index for power-law model.

^cLogarithm of the fraction f of the disk blackbody emission which is scattered for the BM model.

^dNormalization of the BM model.

^eEffective neutral hydrogen absorbing column density.

^f χ^2 value for the fit and number of degrees of freedom (no. spectral bins - no. of fit parameters).

Table 11. Additional Notes on Sample of Nearby Galaxies

Galaxy Name	Other Name	X-ray Source? ^a	Class ^b	Ref. ^b	M_{\bullet}^c $\log M_{\odot}$	Ref. ^c	Notes ^d
NGC 205	M110	no		
NGC 221	M32	yes	...		6.5	1,2	
NGC 300		no		
NGC 598	M33	yes	H II	1	...		
NGC 1313		yes	H II	2	...		
NGC 1396		no		
AM 0337-353		no		
IC 342		yes	H II	1	...		
NGC 1705		no	H II	3	...		SB ref 1, NED H II
NGC 2403		yes	H II	1	...		
Ho II		yes		normal ref 2
ESO 495-G21	He 2-10	yes		PN-like galaxy NED notes
UGC 5086		no		dwarf
NGC 3031	M81	yes	S1.5,LINER	1,2	...		
Ho IX		no		dwarf
Leo A		no		dwarf
NGC 3990		no		
NGC 4138		no	S1.9	1	...		
NGC 4150		yes		
NGC 4190		yes		
UGCA 276	DDO 113	no		
UGC 7356		no		
NGC 4278		yes	L1.9,Sy1	1,3	9.2	2	
NGC 4286		no		

Table 11—Continued

Galaxy	Other	X-ray	Class ^b	Ref. ^b	M_{\bullet} ^c	Ref. ^c	Notes ^d
Name	Name	Source? ^a			$\log M_{\odot}$		
NGC 4374	M84	yes	L2	1	9.2	3	
IC 3303		no		
NGC 4387		no		
NGC 4406	M86	yes		
NGC 4449		yes	H II	1,2	...		SB ref 2
NGC 4485		yes	H II	1	...		
IC 3540		no		
NGC 4552	M89	yes	T2:	1	8.7	2	
NGC 4569	M90	yes	T2,LINER	1,2	...		
NGC 4627		no		
NGC 5204		yes	H II	1	...		
NGC 5408		yes		
NGC 6822		yes		
NGC 6946		yes	H II	1	...		
NGC 7320		no		

^aWas a compact X-ray source found in the current paper?

^bNuclear optical spectrum classification. References: (1) Ho, Filippenko & Sargent 1995; (2) Kinney et al. 1993; (3) NED

^cCentral Dark Mass as determined by dynamical means. References: (1) Bender et al. 1996; (2) Magorrian et al. 1998; (3) Bower et al. 1998

^dNotes on galaxies. References: (1) Lamb et al. 1985; (2) Kinney et al. 1993

Table 12. Unabsorbed X-ray Luminosities of Central X-ray Sources

Galaxy Name	$F(2-10 \text{ keV})^a$ ($\text{erg s}^{-1} \text{ cm}^{-2}$)	$L_X(2-10 \text{ keV})^b$ (erg s^{-1})
M33 # 1	1.02×10^{-11}	5.98×10^{38}
M33 # 2	1.11×10^{-11}	6.51×10^{38}
NGC 1313 #1	1.86×10^{-12}	3.05×10^{39}
NGC 1313 #2	1.06×10^{-12}	1.74×10^{39}
NGC 5408	6.36×10^{-13}	1.83×10^{39}
NGC 4374	6.86×10^{-13}	2.32×10^{40}
NGC 4406	5.42×10^{-13}	1.83×10^{40}
NGC 4552	5.73×10^{-13}	1.94×10^{40}

^aUnabsorbed 2–10 keV flux for: total model (spiral galaxies M33, NGC 1313 and NGC 5408) or hard component (elliptical galaxies (NGC 4374, NGC 4406 and NGC 4552).

^bX-ray luminosities for the fluxes given in column 2 and the distances given in Table 3?

REFERENCES

Antonucci, R. R. J. 1993, *ARA&A*, 31, 473

Beckman, J., Cepa, J., Prieto, M., & Tunon, C. M. 1987, *Rev. Mex. Astron. Astrof.*, 14, 134

Belloni, T., Mendez, M., King, A. R., van der Klis, M., & van Paradijs, J. 1997, *ApJ*, 488, L109

Bender, R., Kormendy, J., & Dehnen, W. 1996, *ApJ*, 464, L123

Bothun, G. D. 1986, *AJ*, 91, 507

Bower, G. A. et al. 1998, *ApJ*, 492, L111

Bridle, A. H., & Perley, R. A. 1984, *ARA&A*, 22, 319

Briel, U. G., et al. 1996, ROSAT User's Handbook (December 1996 HTML test version – http://ftp.rosat.mpe-garching.mpg.de/rosat_svc/doc/handbook/html)

Brown, G. E., & Bethe, H. A. 1994, *ApJ*, 423, 659

Buta, R., Mitra, S., de Vaucouleurs, G., & Corwin, H. G. 1994, *AJ*, 107, 118

Canizares, C. R., Fabbiano, G., & Trinchieri, G. 1987, *ApJ*, 312, 503

Cavaliere, A., & Padovani, P. 1988, *ApJ*, 333, L33

Chevalier, R., & Fransson, C. 1994, *ApJ*, 420, 268

Colbert, E. J. M., Petre, R., Schlegel, E. M., & Ryder, S. D. 1995, *ApJ*, 446, 177

Dekel, A., & Silk, J. 1986, *ApJ*, 303, 39

Dickey, J. M., & Lockman, F. J. 1990, *ARA&A*, 28, 215

Di Matteo, T., & Fabian, A. C. 1997, *MNRAS*, 286, L50

de Vaucouleurs, G., de Vaucouleurs, A., Corwin, H. G., Buta, R. J., Paturel, G., & Fouque, P. 1991, Third Reference Catalog of Bright Galaxies (RC3; New York: Springer-Verlag)

Ebisawa, K., Titarchuk, L., & Chakrabarti, S. K. 1996, PASJ, 48, 59

Elvis, M. et al. 1994, ApJS, 95, 1

Eskridge, P. B., White, R. E., III, & Davis, D. S. 1996, ApJ, 463, L59

Ford, H. C., et al. 1994, ApJ, 435, L27

Forman, W., Jones, C., David, L., Franx, M., Makishima, K., Ohashi, T., Tucker, W. 1993, ApJ, 418, L55

Forman, W., Jones, C., & Tucker, W. 1985, ApJ, 293, 102

Forman, W., Schwartz, J., Jones, C., Liller, W., & Fabian, A. 1979, ApJ, 234, L27

Fullmer, L., & Lonsdale, C. 1989, Cataloged Galaxies and Quasars in the IRAS Survey (JPL Pub. D-1932, Version 2, Appendix B)

Gammie, C. F., Narayan, R., & Blandford, R. 1999, ApJ, submitted (astro-ph/9808036)

Greiner, J. 1996, A&AS, 120, 239 (Special Issue: Third Compton Symp.)

Harms, R. J., et al. 1994, ApJ, 435, L35

Harmon, B. A. et al. 1997, ApJ, 477, L85

Heckman, T. M. 1980, A&A, 87, 152

Herrnstein, J. R., Greenhill, L. J., Moran, J. M., Diamond, P. J., Inoue, M., Nakai, N., & Miyoshi, M. 1998, ApJ, 497, L69

Ho, L. C., Filippenko, A. V., & Sargent, W. L. W. 1995, ApJS, 98, 477

Hummel, E., Sancisi, R., & Ekers, R. D. 1984, A&A, 133, 1

Ishisaki, Y. et al. 1996, PASJ, 48, 237

Johansson, L. 1987, *A&A*, 182, 179

Kinney, A. L., Bohlin, R. C., Calzetti, D., Panagia, N., & Wyse, R. F. G. 1993, *ApJS*, 86, 5

Kormendy, J., & Richstone, D. 1995, *ARA&A*, 33, 581

Lamb, S. A., Gallagher, J. S., Hjellming, M. S., & Hunter, D. A. 1985 *ApJ*, 291, 63

Lasota, J.-P., Abramowicz, M. A., Chen, X., Krolik, J., Narayan, R., & Yi, I. 1996, *ApJ*, 462, 142

Lira, P., Lawrence, A., & Johnson, R. A. 1998, in proceedings of 32nd COSPAR Scientific Assembly Session E1.2 (“The AGN-Normal Galaxy Connection”), eds. A. Kinney, L. Ho, & H. Schmitt

Loewenstein, M., Hayashida, K., Toneri, T., & Davis, D. S. 1998, *ApJ*, in press (April)

Mahadevan, R. 1997, *ApJ*, 477, 585

Magorrian, J. et al. 1998, *AJ*, 115, 2285

Matsumoto, H., Koyama, K., Awaki, H., Tsuru, T., Loewenstein, M., & Matsushita, K. 1997, *ApJ*, 482, 133

Matsushita, K., et al. 1994, *ApJ*, 436, L41

Melisse, J. P. M., & Israel, F. P. 1994, *A&A*, 285, 51

Miyoshi, M., Moran, J., Herrnstein, J., Greenhill, L., Nakal, N., Diamond, P., & Inoue, M., 1995, *Nature*, 373, 127

Moshir, et al. 1990, IRAS Faint Source Catalog, version 2

Nandra, K., George, I. M., Mushotzky, R. F., Turner, T. J., & Yaqoob, T. 1997, *ApJ*, 477, 602

Narayan, R. 1997, in Accretion Phenomena and Related Outflows (IAU Colloq. 163, ASP Conf. Ser. Vol. 121), eds. D. Wickramasinghe, L. Ferrario, & G. Bicknell, p. 75

Narayan, R., & Yi, I. 1994, *ApJ*, 428, L13

Narayan, R., & Yi, I. 1995a, *ApJ*, 444, 231

Narayan, R., & Yi, I. 1995b, *ApJ*, 452, 710

Okada, K., Dotani, T., Makishima, K., Mitsuda, K., & Mihara, T. 1998, *PASJ*, 50, 25

Okada, K., Mihara, T., Makishima, K., & The ASCA Team 1994, in *New Horizon of X-ray Astronomy* (Universal Academy Press) (eds. Makino, F., & Ohashi, T.), p. 515

Osterbrock, D. E. 1989, in *Astrophysics of Gaseous Nebulae and Active Galactic Nuclei* (Mill Valley: University Science), p. X

Petre, R., Mushotzky, R. F., Serlemitsos, P. J., Jahoda, K., & Marshall, F. E. 1993, *ApJ*, 418, 644

Petre, R., Okada, K., Mihara, T., Makishima, K., & Colbert, E. J. M. 1994, *PASJ*, 46, L115

Ptak, A., Serlemitsos, P., Yaqoob, T., & Mushotzky, R. 1998, *ApJS*, in press for January 1999 issue

Raymond, J. C., & Smith, B. W. 1977, *ApJS*, 35, 419

Reynolds, C. S., Di Matteo, T., Fabian, A. C., Hwang, U., & Canizares, C. R. 1996, *MNRAS*, 283, L111

Sandage, A., & Hoffman, G. L. 1991, *ApJ*, 379, L45

Schlegel, E. M. 1995, *Rep. Prog. Phys.*, 58, 1375

Schlegel, E. M., Petre, R., & Colbert, E. J. M. 1996, *ApJ*, 456, 187

Shakura, N. J., & Sunyaev, R. A. 1973, *A&A*, 24, 337

Shrader, C., & Titarchuk, L. 1998, *ApJ*, 499, L31

Silk, J., & Rees, M. J. 1998, *A&A*, 331, L1

Takano, M., Mitsuda, K., Fukazawa, Y., & Nagase, F. 1994, *ApJ*, 436, L47

Tanaka, Y. 1989, in Two Topics in X-ray Astronomy (23rd ESLAB Symp.), eds. J. Hunt & B. Battrick (Paris: ESA), p. 3

Tanaka, Y., & Lewin, W. H. G. 1995, in X-ray Binaries (ed. Lewin, Paradijs, & van den Heuvel), Ch. 3

Thornley, M. D. 1996, ApJ, 469, L45

Tully, R. B. 1988, Nearby Galaxies Catalog (Cambridge: Cambridge Univ. Press)

Turner, T. J., George, I. M., Nandra, K., & Mushotzky, R. F. 1997, ApJS, 113, 23

Wandel, A. 1991, A&A, 241, 5

Wrobel, J. M., & Heeschen, D. S. 1984, ApJ, 287, 41

Yaqoob, T., Ebisawa, K., & Mitsuda, K. 1993, MNRAS, 264, 411

Zhang, S. N. et al. 1997, ApJ, 479, 381

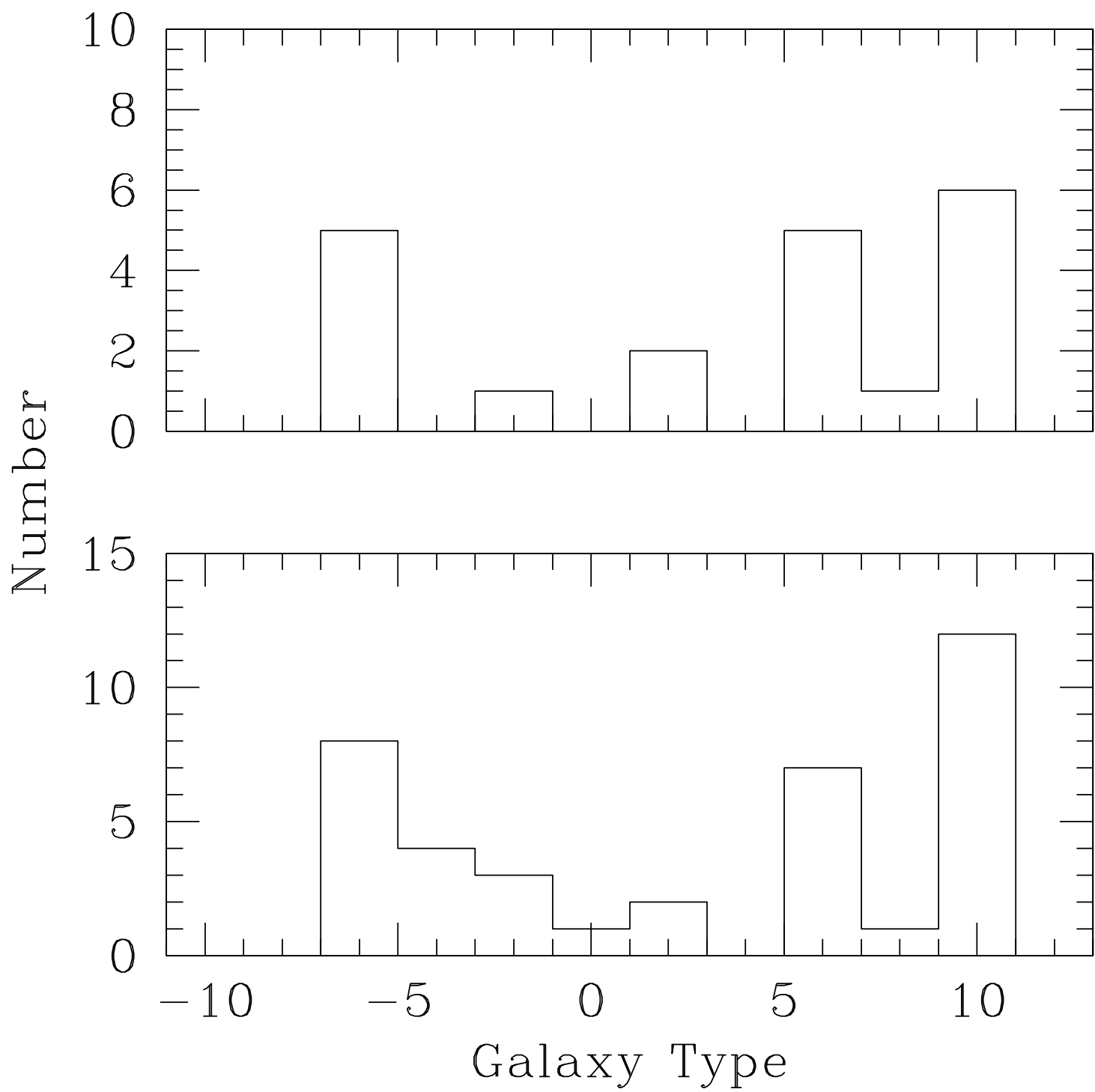
Fig. 1.— Histogram of Galaxy Type for galaxies with detected X-ray sources (upper panel) and galaxies in entire sample (lower panel). For clarity, the galaxy ESO 495-G21 (type 90.0) has been omitted from the plot.

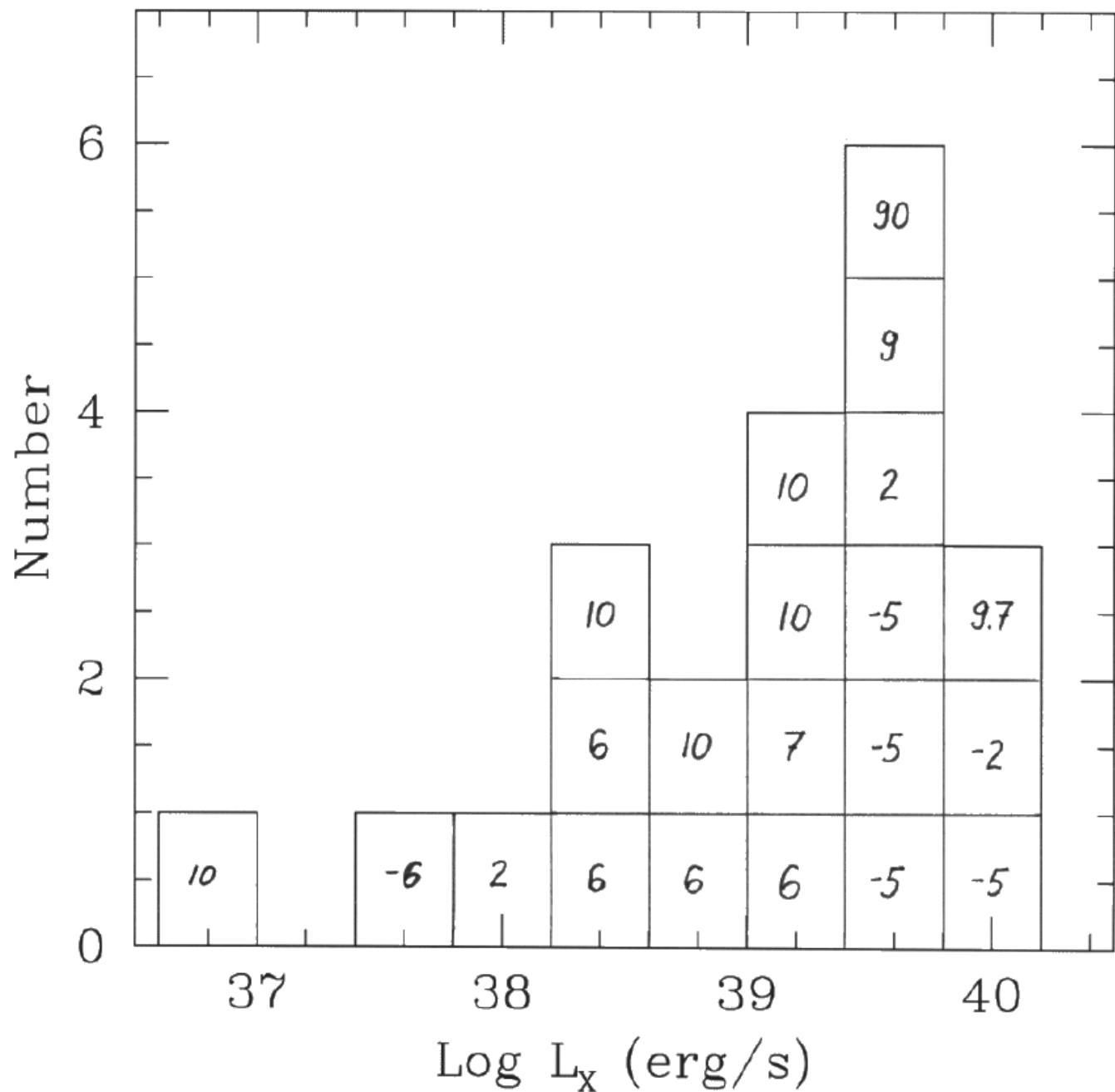
Fig. 2.— Histogram of the 0.2–2.4 keV X-ray luminosity of the compact X-ray sources. Galaxy type for each galaxy is indicated on the plot.

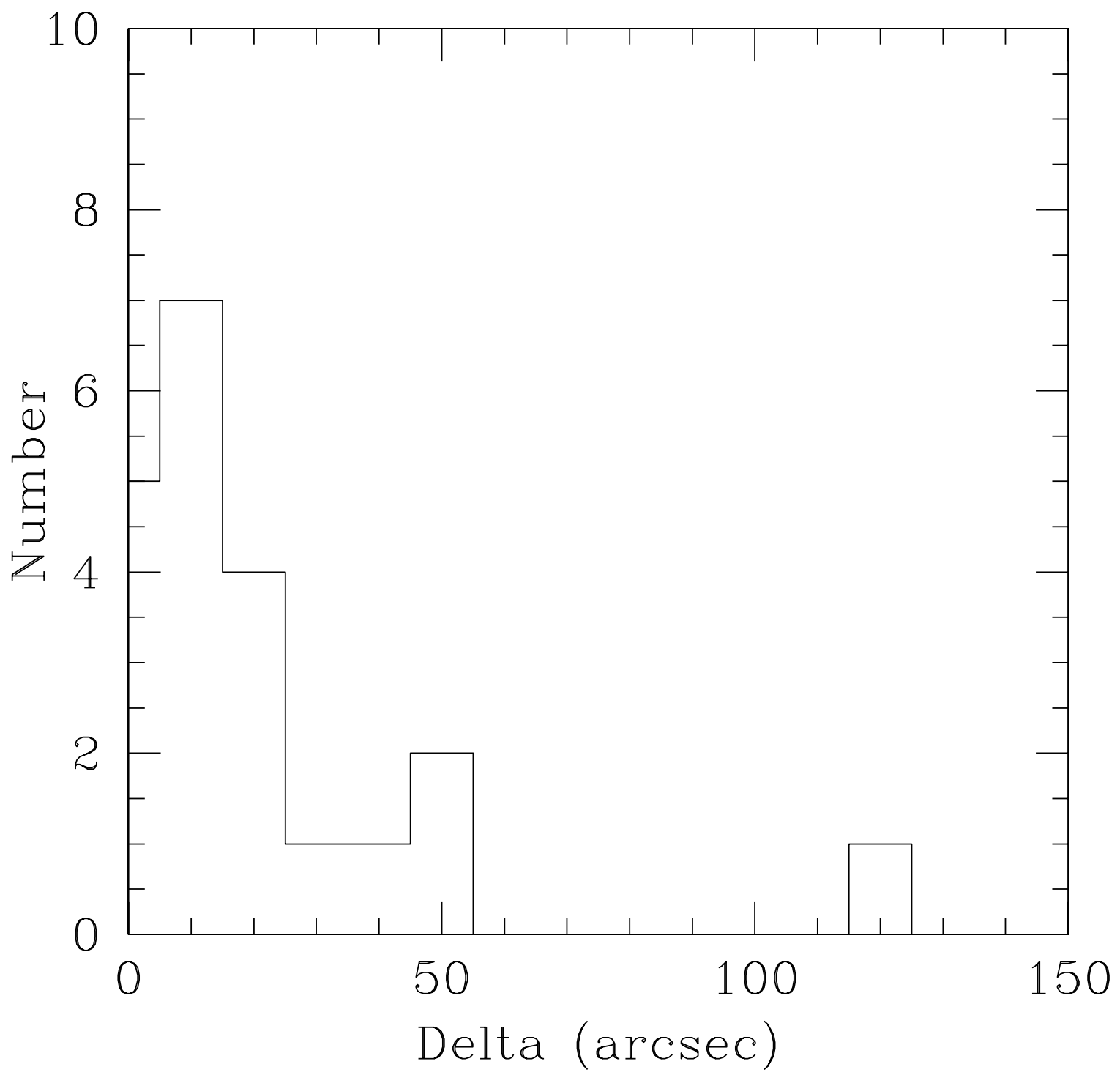
Fig. 3.— Histogram of the separation between the X-ray position of the detected X-ray sources and the photometric center of the galaxy, in units of (a) arcseconds and (b) parsecs.

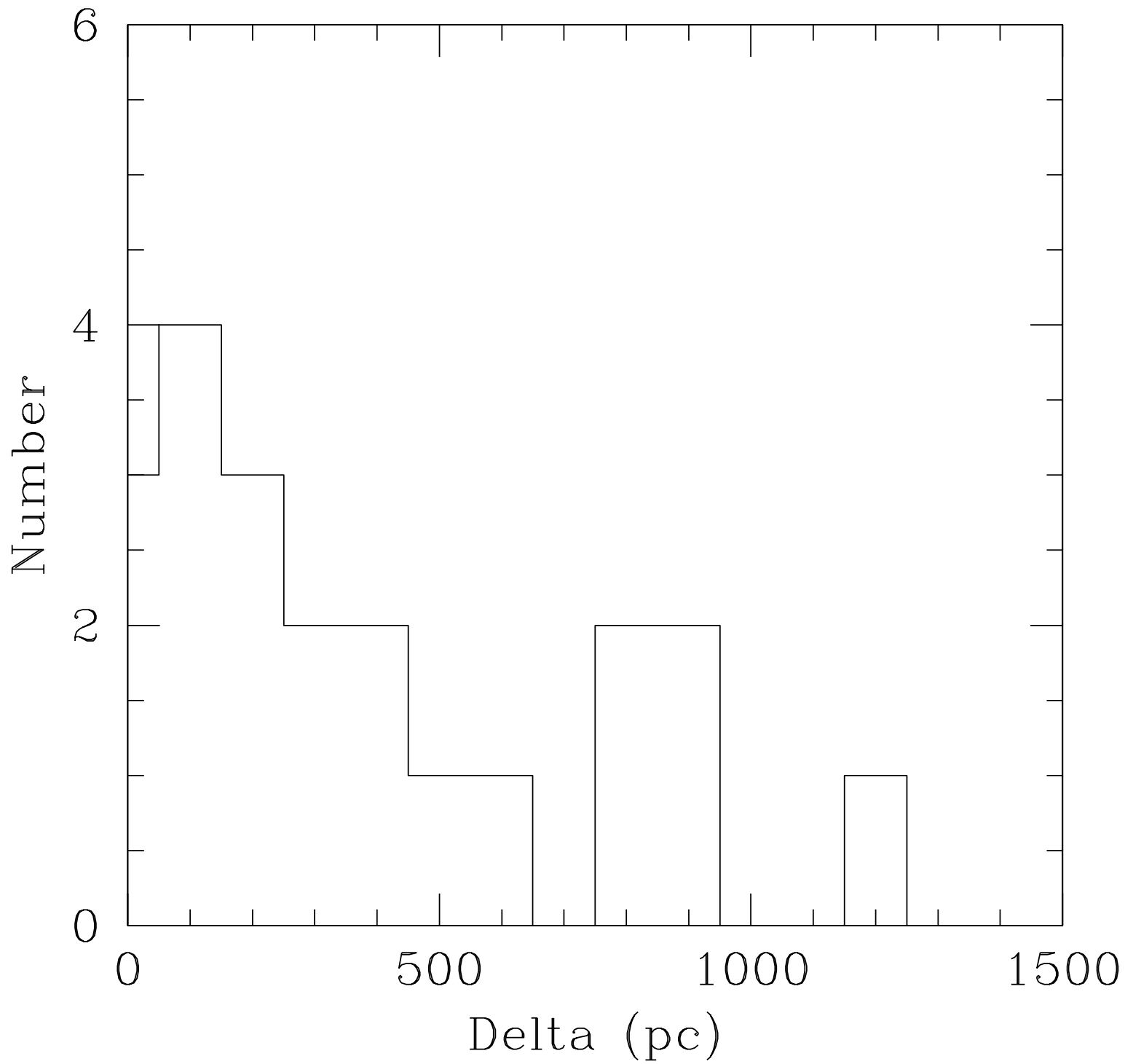
Fig. 4.— Plot of logarithm of the 0.2–2.4 keV X-ray luminosity and the angular separation of the X-ray source from the photometric center. Those galaxies with previous evidence of nuclear activity are labelled as a filled rectangle, while unclassified galaxies are labelled with an open rectangle.

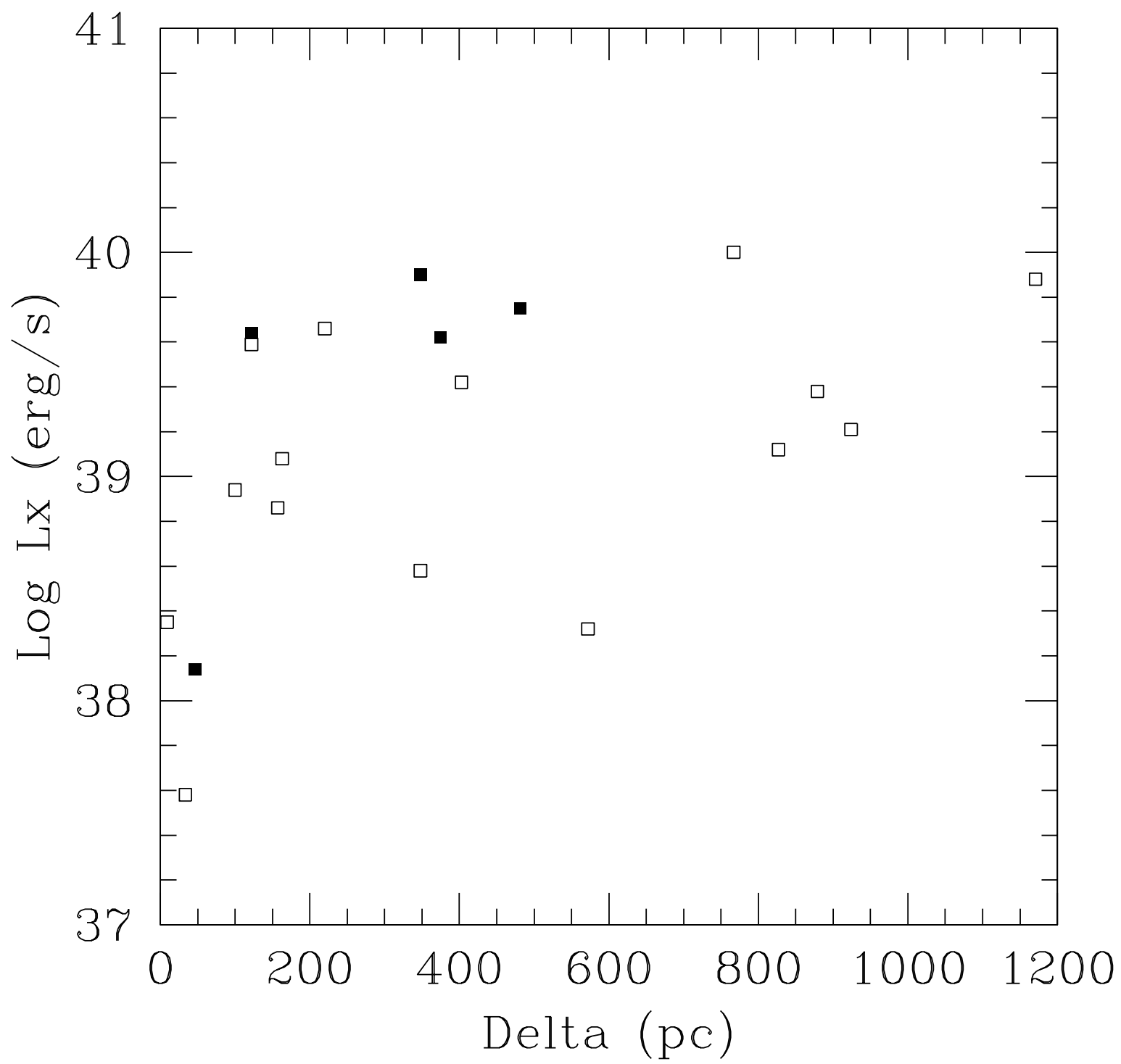
Fig. 5.— Plot of the logarithm of the ROSAT X-ray luminosity and the blue luminosity (from Tables 5 and 1, respectively). Elliptical galaxies are labelled as filled rectangles, spiral galaxies are labelled as filled triangles, and dwarf and irregular galaxies are labelled as open triangles. The solid line marks the predicted X-ray luminosity of X-ray binaries (from Canizares et al. 1987) for early-type galaxies.











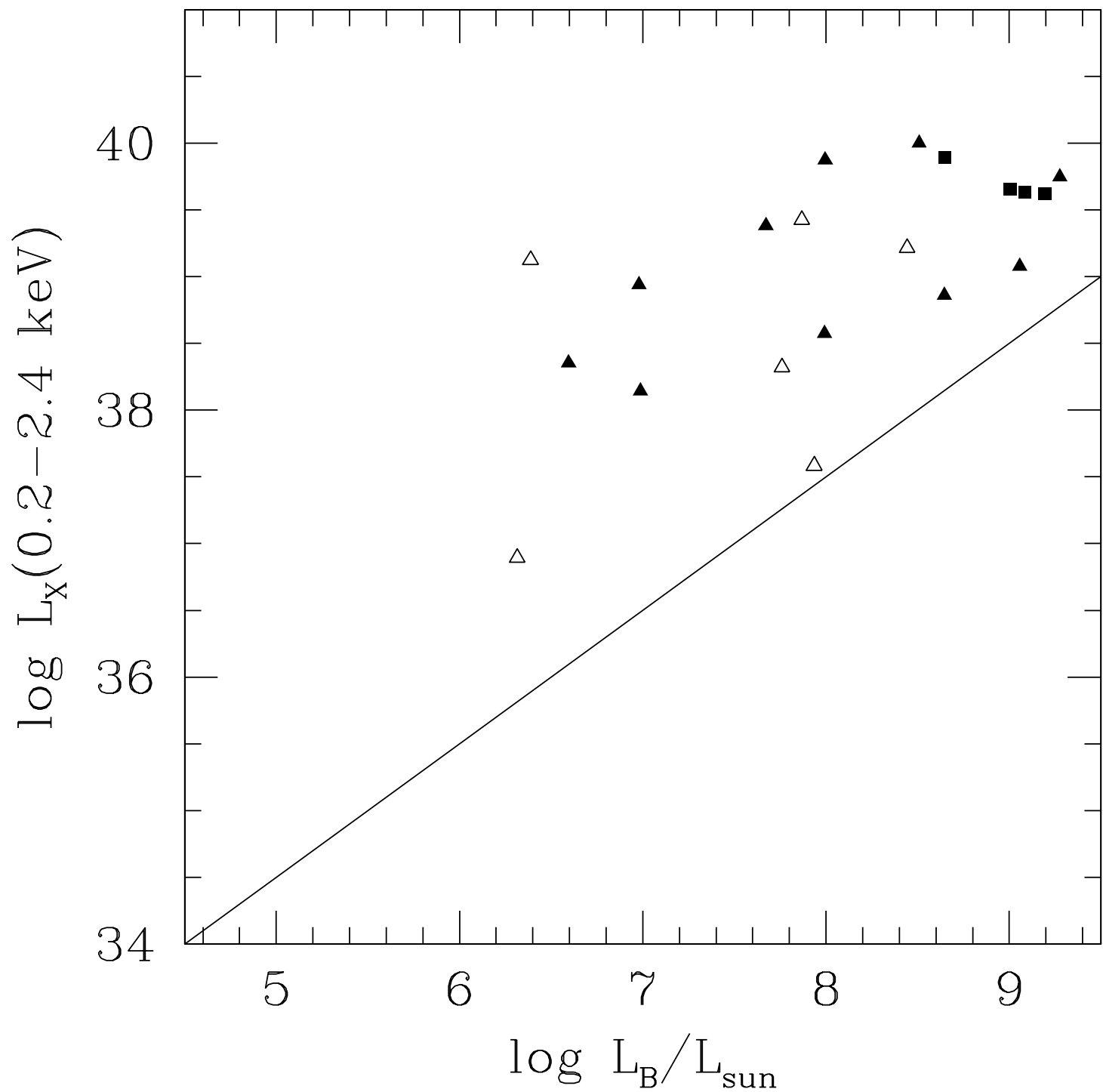


TABLE 7
TWO-COMPONENT FITS TO ASCA DATA

Galaxy Name	Model ^a	kT or kT _{in} ^b (keV)	Normalization ^c	F ^d	Normalization ^c	N _H ^e (10 ²¹ cm ⁻²)	Abundance ^f	χ ² / d.o.f. ^g	F (wrt PL) ^h	F (wrt RS) ^h
Spiral Galaxies										
M33 (#1)	RS+PL	3.66 2.88 – 4.10	8.37 × 10 ⁻³	2.61 2.38 – 2.78	5.23 × 10 ⁻³	6.93 5.83 – 8.51	0 < 0.06	580 / 592	26.9 (>99.9%)	...
	DBB+PL	1.15 1.01 – 1.30	0.281	2.35 1.98 – 2.84	3.06 × 10 ⁻³	1.80 1.06 – 2.56		550 / 593	58.8 (>99.9%)	
M33 (#2)	RS+PL	3.56 2.80 – 3.94	1.11 × 10 ⁻²	2.71 2.45 – 2.96	5.67 × 10 ⁻³	9.79 8.08 – 12.43	0 < 0.12	670 / 673	56.3 (>99.9%)	...
	DBB+PL	1.15 1.05 – 1.26	0.345	2.26 1.87 – 2.69	2.49 × 10 ⁻³	1.25 0.59 – 1.91		630 / 674	111.3 (>99.9%)	
NGC 1313 (#1)	RS+PL	0.65 0.35 – 0.78	1.57 × 10 ⁻³	1.84 1.71 – 1.98	5.60 × 10 ⁻⁴	5.02 0.53 – 9.54	0.03 0.01 – 1.23	233 / 256	4.03 (99.2%)	11.0 (> 99.9%)
	DBB+PL	0.12 0.11 – 0.14	7984	1.97 1.83 – 2.10	6.85 × 10 ⁻⁴	4.76 2.72 – 6.63		233 / 257	6.07 (99.7%)	
NGC 1313 (#2)	RS+PL	0.90 0.84 – 1.06	1.11 × 10 ⁻³	2.74 2.58 – 2.96	1.18 × 10 ⁻³	5.35 3.13 – 8.14	0.08 0.04 – 1.14	177 / 195	2.94 (97%)	10.5 (> 99.9%)
	DBB+PL	1.34 0 – 2.37	8.13 × 10 ⁻³	3.09 2.58 – 4.44	1.30 × 10 ⁻³	3.28 2.13 – 5.28		184 / 196	0.53 (41%)	
NGC 5408	RS+PL	0.85 0.67 – 1.05	4.31 × 10 ⁻⁵	2.28 2.19 – 2.39	3.67 × 10 ⁻⁴	0 < 0.4	1.0 ⁱ	250 / 267	5.87 (99.7%)	99.3 (> 99.9%)
	DBB+PL	0.13 0.10 – 0.20	1363	2.45 2.25 – 2.65	4.74 × 10 ⁻⁴	2.34 0.39 – 4.2		254 / 267	3.68 (97%)	

TABLE 7—Continued

Galaxy Name	Model ^a	kT or kT _{in} ^b (keV)	Normalization ^c	Γ ^d	Normalization ^c	N _H ^e (10 ²¹ cm ⁻²)	Abundance ^f	χ^2 / d.o.f. ^g	F (wrt PL) ^h	F (wrt RS) ^h
Elliptical Galaxies										
NGC 4374	RS+PL	0.73 0.68 – 0.77	1.88×10^{-3}	2.19 1.81 – 2.68	3.52×10^{-4}	4.16 0.77 – 12.14	0.17 0.11 – 5.0 ^j	229 / 213	67.6 (>99.9%)	66.5 (>99.9%)
	DBB+PL	0.075 0.074 – 0.077	4.02×10^7	3.42 3.21 – 3.62	1.92×10^{-3}	11.6 11.1 – 12.1		261 / 214	76.3 (>99.9%)	
NGC 4406	RS+PL	0.82 0.81 – 0.84	3.84×10^{-4}	3.42 3.11 – 3.76	1.43×10^{-3}	3.48 2.11 – 6.09	5.0 ^j > 0.55	430 / 383	225.3 (>99.9%)	12.9 (>99.9%)
	DBB+PL	0.061 0.060 – 0.062	2.00×10^{10}	5.16 4.97 – 5.34	1.64×10^{-2}	17.5 17.1 – 18.0		545 / 384	226.9 (>99.9%)	
NGC 4552	RS+PL	0.69 0.64 – 0.74	1.16×10^{-4}	2.03 1.64 – 2.39	2.33×10^{-4}	7.71 2.18 – 14.43	1.17 0.57 – 5.0 ^j	243 / 245	54.1 (>99.9%)	106.4 (>99.9%)
	DBB+PL	0.065 0.064 – 0.067	3.22×10^8	2.70 2.49 – 2.93	6.14×10^{-4}	14.8 14.1 – 15.6		263 / 246	65.9 (>99.9%)	

NOTE: Ranges for parameters are given for 90% confidence for one interesting parameter ($\Delta\chi^2 = 2.7$).

^aEmission model used in the spectral fit: RS = Raymond-Smith thermal plasma model, PL = power-law model, and DBB = multicolor disk blackbody model.

^bGas temperature kT for Raymond-Smith plasma model, or surface temperature of inner radius of accretion disk (kT_{in}).

^cNormalization for the RS, PL and DBB models. Units for the RS and PL models are as described in the notes to Table 5. Units for the DBB model are R_{in}(km)² cos θ / D(10 kpc)², where R_{in}(km) is the inner radius of the accretion disk in units of km, cos θ is the cosine of the inclination of the accretion disk from the line of sight, and D(10 kpc) is the distance to the source in units of 10 kpc.

^dPhoton index of power-law model.

^eEffective neutral hydrogen absorbing column density.

^fAbundance of metals in the thermal plasma, relative to cosmic abundances.

^g χ^2 value for the fit and number of degrees of freedom (no. spectral bins - no. of fit parameters).

^hF statistic for the fit, in comparison to the PL or RS model from Table 5. Here F = $(\Delta\chi^2/n)/\chi^2_\nu$, where n is the difference in the number of parameters and χ^2_ν is the reduced χ^2 value for the fit with the larger number of fit parameters. In parenthesis is the significance of the given F value.

ⁱAbundance was unconstrained between 0 and 5.0 (times cosmic values) and so was fixed at a value of 1.0.

^jAbundance pegged at upper limit of 5.0.

TABLE 8
THREE-COMPONENT FITS TO ELLIPTICAL GALAXY ASCA SPECTRA

Galaxy Name	kT ^a (keV)	Norm ^b	kT _{in} ^c (keV)	Norm ^b	Γ ^d	Norm ^b	N _H ^e (10 ²¹ cm ⁻²)	Abundance ^f	χ^2 / d.o.f. ^g	F (wrt DBB+PL) ^h	F (wrt RS+PL) ^h
NGC 4374	0.74	1.92×10^{-3}	0.45	0.9905	1.8 ⁱ	1.79×10^{-4}	8.63	0.18	226 / 212	16.4	2.81
	0.68 – 0.78		0.29 – 0.77				< 18.2	0.11 – 0.24		(>99.9%)	(90%)
NGC 4406	0.82	1.96×10^{-3}	0.14	18500	3.43	1.51×10^{-3}	14.1	0.99	428 / 381	34.7	0.89
	0.80 – 0.84		0.09 – 0.34		0.95 – 4.66		2.9 – 26.6	> 0.50		(>99.9%)	(59%)
NGC 4552	0.70	7.24×10^{-5}	0.51	0.2770	1.68	1.29×10^{-4}	9.09	1.95	242 / 243	7.03	0.50
	0.65 – 0.75		0 – 1.21		0.92 – 2.40		0.50 – 26.2	> 0.29		(>99.9%)	(39%)

NOTE: Ranges for parameters are given for 90% confidence for one interesting parameter ($\Delta\chi^2 = 2.7$).

^a Plasma temperature for Raymond-Smith component.

^b Normalization values for models. Units are as stated in the notes to Tables 4 and 5.

^c Surface temperature of the disk at the innermost radius (for the multicolor disk blackbody component).

^d Photon index for power-law model.

^e Effective neutral hydrogen absorbing column density.

^f Abundance of metals in the thermal plasma, relative to cosmic abundances.

^g χ^2 value for the fit and number of degrees of freedom (no. spectral bins - no. of fit parameters).

^h F statistic for the fit, in comparison to the DBB+PL or RS+PL model from Table 5. In parenthesis is the significance of the given F value.

ⁱ Abundance was unconstrained between 0 and 5.0 (times cosmic values) and so was fixed at a value of 1.0.

^j Spectral index was not well constrained, so was fixed at $\Gamma = 1.8$.